



Evolution of auroral substorm as viewed from MHD simulations: dynamics, energy transfer and energy conversion

Yusuke Ebihara¹ · Takashi Tanaka²

Received: 17 June 2019 / Accepted: 22 December 2019 / Published online: 11 January 2020
© The Author(s) 2020

Abstract

An auroral substorm is a visual manifestation of large-scale, transient disturbances taking place in space surrounding the Earth, and is one of the central issues in the space plasma physics. While a number of studies have been conducted, a unified picture of the overall evolution of the auroral substorm has not been drawn. This paper is aimed to overview the recently obtained results of global magnetohydrodynamics (MHD) simulations in a context of a priori presence of anomalous resistivity leading to magnetic reconnection, and to illuminate what the global MHD simulation can sufficiently reproduce the auroral transients during the auroral substorm. Some auroral transients are found to be seamlessly reproduced by the MHD simulation, including complicated auroral structures moving equatorward during the growth phase, auroral brightening starting to appear near the equatorward border of the preexisting auroral arc, and an auroral surge traveling westward. Possible energy transfer and conversion from the solar wind to the Earth are also overviewed on the basis of the MHD simulation. At least, 4 dynamo regions appear sequentially in the course of the development of the auroral substorm. Although the MHD simulation reproduces some transients, further studies are needed to investigate the role of kinetic processes.

Keywords Magnetosphere · Auroral substorm · Simulation · Solar wind–magnetosphere–ionosphere coupling · MHD simulation

✉ Yusuke Ebihara
ebihara@rish.kyoto-u.ac.jp

¹ Research Institute for Sustainable Humanosphere, Kyoto University, Gokasho, Uji, Kyoto 611-0011, Japan

² Kyushu University, Motoooka 744, Nishi-ku, Fukuoka 819-0395, Japan

1 Introduction

An auroral substorm is a noticeable phenomenon in the polar region on the night-side. Suddenly, bright aurorae appear on a pre-existing (faint) auroral oval, and expand quickly (Akasofu 1964). An example of the auroral substorm is shown in Fig. 1. Simultaneously, a large amount of electric current flows horizontally in the ionosphere at ~ 100 -km altitude, which is called an auroral electrojet. The auroral electrojet causes magnetic disturbances on the ground in the polar region, and gives rise to Joule dissipation reaching $\sim 10^{11}$ W (Ahn et al. 1983; Kamide et al. 1996; Østgaard 2002; Palmroth et al. 2005; Richmond et al. 1990; Rostoker et al. 1980; Tanskanen et al. 2002; Zhou et al. 2011). Observations have shown that the electrojet is connected to the field-aligned currents (FACs) intensified during the auroral expansion (Atkinson 1967; Boström 1964; Connors et al. 2014; Frank et al. 1982; Kamide et al. 1981; Kamide and Akasofu 1975; Rostoker et al. 1975). There are two important aspects of the FACs. First, they efficiently supply magnetic energy to the ionosphere along a magnetic field line. Secondly, earthward acceleration of the electrons, which cause bright aurora, is embedded in the upward FAC region. Thus, understanding the generation of the FACs is one of the keys in the study of the auroral substorm.

Figure 2 provides a schematic drawing of possible space environment surrounding the Earth during the auroral expansion. The solar wind, which mostly consists of protons, helium ions and electrons, blows from the Sun to interplanetary space. The magnetic field lines are also swept away from the Sun. The stream of the solar wind is supersonic, so that a bow shock forms in front of the magnetosphere where the intrinsic magnetic field of the Earth dominates. Due to the Earth's intrinsic magnetic field, the solar wind stream is deflected outward (as indicated by the blue line in Fig. 2). The cavity where the Earth's intrinsic magnetic field dominates is called a magnetosphere. The boundary between the solar wind and the magnetosphere is called a magnetopause. The stream of the magnetic energy (Poynting flux) is concentrated to the magnetosphere (as indicated by the red line in Fig. 2). This has been pointed out by Lockwood and Davis (1999) and Papadopoulos et al. (1999). The lobe is the region where the magnetic field lines are open. The plasma sheet, where the plasma pressure is relatively high, forms near the equatorial plane in the tail region. The cross-tail current flowing in the plasma sheet and the magnetopause sustains the structure of the tail.



Fig. 1 Evolution of auroral substorm observed by the Polar satellite (Courtesy of NASA and University of Iowa)

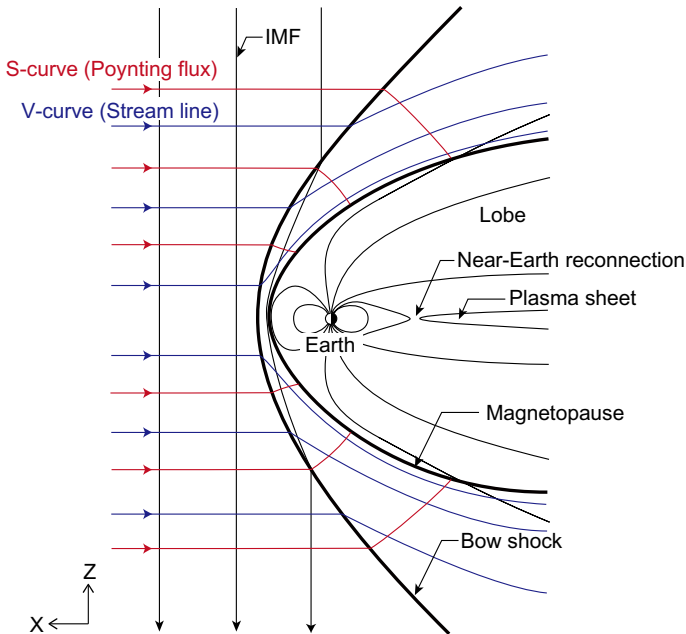


Fig. 2 Schematic drawing of the magnetosphere during the substorm expansion. The interplanetary magnetic field (IMF) looks southward (negative z direction). Magnetic reconnection takes place in the day-side magnetopause, and near-Earth plasma sheet. The red line indicates an integral curve of the Poynting flux. The blue line indicates an integral curve of the velocity, that is, a stream line of plasma (After Ebihara et al. 2019)

The auroral substorm (manifested by the evolution of aurora) is basically an ionospheric phenomenon, but it is regarded as a consequence of drastic disturbances in the magnetosphere. In that sense, the chain reaction and the energy transfer from the solar wind to the ionosphere must be studied to understand the auroral substorm. The global magnetohydrodynamics (MHD) simulation is still a useful tool to investigate the chain reaction and the energy transfer in spite of inherent limitations as mentioned below.

2 Observation

2.1 Evolution of auroral substorm

A number of studies have been conducted to understand the auroral substorm and the associated processes taking place in the magnetosphere. The following is a brief summary of past observations related to the auroral transients and energy transfer. Regarding the onset processes, readers may refer to Baker et al. (1996) and Lui (1996).

2.1.1 Northward IMF

When the interplanetary magnetic field (IMF) is northward, the magnetosphere and the ionosphere are calm. Faint, and relatively stable aurorae, including sun-aligned arcs, are observed at high latitudes (Davis 1962; Eliasson et al. 1987; Frank et al. 1982; Ismail et al. 1977; Lassen and Danielsen 1978; Meng and Lundin 1986; Newell et al. 1997; Shiokawa et al. 1995, 1997b).

2.1.2 Growth phase

The growth phase starts when IMF turns southward. Longitudinally elongated auroral arcs gradually move equatorward (Akasofu 1964). The speed of the arc is 2–6 km/min at the ionospheric altitude (Haerendel et al. 2012; Lassen and Sharber 1977). The thickness of the quiet arc is ~100 km on the basis of satellite observations (Johnson et al. 1998). The thickness of ~100 km is probably the upper limit because of the relatively coarse resolution of satellite-borne imaging. The ground-based observations have shown that the thickness is ~3.5 km at 200-km altitude (Dahlgren et al. 2009). The arcs are called evening anticorrelation arcs (Marklund 1984), growth phase arcs (Haerendel 2010; Lyons et al. 2011; Nishimura et al. 2012), preexisting arcs (Jiang et al. 2012), and quiet evening arcs (Coroniti and Pritchett 2014). Hereinafter, we refer it to as a quiet arc. Multiple quiet arcs tend to form within the auroral oval before the onset of the substorm expansion (Akasofu 1964; Haerendel et al. 2012).

The quiet arcs are caused by precipitation of electrons with a peak energy of 1–5 keV (Lassen and Sharber 1977; Meng 1976). The electrons are supposed to be accelerated by an ‘inverted-V’ type quasi-static upward electric fields (Jiang et al. 2012, 2015; Lessard et al. 2007; Meng 1976). The ‘inverted-V’ is a structure seen in an energy versus time spectrogram of precipitating electrons obtained by a low-altitude satellite. The peak energy of precipitating electrons increases, and decreases as the satellite travels in the horizontal direction. A monochromatic energy component is referred to as the presence of quasi-DC electric field parallel to the magnetic field line. Readers may refer to Lin and Hoffman (1982) for details of the ‘inverted-V’. On the duskside, the parallel electric field is clearly accompanied with upward FACs (Jiang et al. 2012; Korth et al. 2014; Mozer et al. 1980; Swift 1981). The field-aligned current density follows ‘inverted-U’, rather than ‘inverted-V’, suggesting spatial dependence of parallel conductivity (Sakanoi et al. 1995). The parallel electric field is located at altitudes below 3.0–3.5 R_E (Mozer and Hull 2001).

Magnetic merging of the southward component of the IMF with the Earth’s magnetic field on the dayside magnetosphere gives rise to enhancement of the convection (Dungey 1961; Nishida and Kamide 1983). As a consequence of the stimulation of the convection, the magnetic field in the lobe region increases and the plasma sheet becomes thin (Fairfield and Ness 1970; McPherron 1972; Nishida and Fujii 1976; Nishida and Hones 1974). The thinning of the tail current sheet is suggested to roughly explain the equatorward expansion of the auroral oval (Sergeev et al. 1990).

Some kinds of meso-scale auroral structures, known as quiet arcs, and north–south and east–west aligned arcs, persist during the growth phase. These arcs are fairly stable. One idea is that the quiet arc is a projection of inhomogeneous plasma pressure distribution near the equatorial plane (Antonova 1993; Coroniti and Pritchett 2014; Haerendel 2007; Lyons and Samson 1992; Stepanova et al. 2002). For the steady-state condition ($\partial/\partial t=0$), misalignment between the pressure gradient and the magnetic gradient gives rise to the generation of FACs (Sato and Iijima 1979). The multiple quiet arcs are also suggested to be caused by the magnetosphere–ionosphere coupling, such as cross-field instability (Ogawa and Sato 1971), feed-back instability (Hasegawa et al. 2010; Lysak and Song 2002; Sato 1978; Watanabe et al. 1986), field-line resonance (Lotko et al. 1998; Rankin et al. 1999; Streltsov and Lotko 1995), and nonlinear evolution of Alfvén waves (Lysak and Dum 1983). Another explanation for the cause of the quiet arcs is pitch angle scattering of electrons in a magnetic field line with a small curvature radius (Yahnin et al. 1997). In this case, the upward FAC is caused by the scattered electrons moving toward the Earth (Sergeev et al. 2011).

A diffusive auroral patch and a discrete auroral form are observed at 630.0 nm and 557.7 nm, respectively, poleward of the auroral oval (Kepko et al. 2009). They are sometimes north–south aligned, or east–west aligned (Nishimura et al. 2010a). The north–south, or east–west aligned arcs are thought to belong to the closed magnetic field line, and to be a projection of an earthward traveling flow burst in the plasma sheet (Kepko et al. 2009; Lyons et al. 2010; Mende et al. 2011; Nishimura et al. 2010a, b). The flow burst is frequently observed in the plasma sheet. The flow burst is called a bursty bulk flow (BBF), and is thought to be a consequence of the near-Earth reconnection (Angelopoulos et al. 1994; Baumjohann et al. 1989). If the plasma content in a flux tube in the flow burst is lower than ambient (known as plasma bubble), FACs will appear at the edges of the flow burst from the requirement of current continuity (Pontius and Wolf 1990; Sergeev et al. 2000). It seems from observation that when the north–south, or east–west aligned aurorae arrive at one of the preexisting quest arcs (or proton aurora), the expansion phase begins. This observational tendency leads to scientists to consider that the arrival of the north–south, or east–west aligned aurorae are closely related to the expansion onset (Kadokura et al. 2002; Lyons et al. 2010; Nishimura et al. 2010a; Oguti 1973).

2.1.3 Expansion phase

Bright aurora sporadically appears in one of the longitudinally elongated auroral arcs (Akasofu 1964). Occasionally, the sudden brightening of aurora is preceded by longitudinally and latitudinally elongated arcs moving equatorward (Kadokura et al. 2002; Kepko et al. 2009; Lyons et al. 2010; Nishimura et al. 2010b; Oguti 1973). The brightening of the aurora is usually accompanied by distinct ray structures, which are also known as beads and optical wave-like structures (Henderson 2009; Liang et al. 2007; Rae et al. 2010; Sakaguchi et al. 2009). Since the spatial wavelength of the beads and the optical wave-like structures is of the order of an ion gyroradius, kinetic effects are thought to be involved (Nishimura et al. 2016). A few minutes later, the bright aurora expands poleward, westward and eastward (Akasofu

1964), which is called a bulge. Ieda et al. (2018) argue the definition of the expansion onset by comparing auroral images obtained by ground-based instruments and those obtained by satellites.

The aurora becomes extremely bright near the leading edge of the bulge. This is called a surge, or a westward traveling surge (WTS) (Akasofu 1963, 1965; Anger et al. 1973; Elphinstone et al. 1995a). The WTS is caused by the intense ‘inverted-V’ precipitation of electrons with peak energy > 10 keV (Cummer et al. 2000; Fujii et al. 1994; Meng et al. 1978; Olsson et al. 1996; Rème and Bosqued 1973; Shiokawa and Fukunishi 1991). Occasionally, electron precipitation that may be caused by Alfvén waves has been observed near the poleward edge of the WTS (Mende 2003; Weimer et al. 1994). Intense upward FACs flows in the poleward part of the WTS (Fujii et al. 1994; Kamide and Akasofu 1975; Marklund et al. 1998; Shiokawa and Fukunishi 1991). Downward FACs are also observed poleward of the WTS (Fujii et al. 1994). Auroral electrojet flows in the ionosphere in association with FACs (Kamide and Akasofu 1975), increasing the Joule dissipation rates in the ionosphere.

Triggering mechanism of the substorm expansion is one of the hottest topics in the substorm study (Angelopoulos et al. 2008). A near-Earth neutral line model has been suggested from early time (Hones et al. 1973; Nishida and Nagayama 1973). The NENL usually takes place first at $16\text{--}20 R_E$ from the center of the Earth at least 2 min before the expansion onset (Miyashita et al. 2009). Intense FACs are generated in the vicinity of the NENL (Treumann et al. 2006), which are supposed to initiate the auroral brightening. If this is the case, auroral breakups will start near the poleward boundary of the auroral oval. This contradicts to the observational fact that the auroral breakup starts near the equatorward boundary of the auroral oval (Elphinstone et al. 1991; Lui and Burrows 1978). A current disruption model resolves this problem (Lui 1996). Cross-field current instability (Lui et al. 1991), and ballooning mode instability (Cheng and Lui 1998; Liu et al. 2012; Roux et al. 1991) are suggested to cause the disruption of the current sheet in the tail region. A hybrid model, which incorporates both the NENL and current disruption models (Baker et al. 1993; Machida et al. 2014), is also proposed. Lui (2011) resurveyed the satellite observations published in the past, and concluded that these observations can be explained in terms of the current disruption. The triggering mechanism has not been settled.

Regardless of the triggering model, a wedge-like current system is supposed to present during the expansion phase (Kepko et al. 2015; McPherron et al. 1973). This current system is called a current wedge, which consists of a downward (earthward) FAC flowing on the dawnside, and an upward (anti-earthward) FAC flowing on the duskside. The counter part of the FACs is believed to be connected to the cross-tail current. In the current disruption model, the current wedge appears where the current disruption takes place in the near-Earth region. This reasonably explains the observational fact that the onset of the auroral expansion occurs near the equatorward boundary of the auroral oval (Lui 1996). The NENL model can also explain the auroral breakups initiating near the equatorward boundary of the auroral oval by incorporating the following processes. Flow shear (vorticity) associated with earthward fast flow originating from the NENL, known as bursty bulk flows (BBFs), can

generate a pair of the FACs (Birn et al. 2004; Birn and Hesse 1991; Keiling et al. 2009; Nakamura et al. 1993). Intrusion of low entropy plasma results in the formation of the FACs due to continuity of the current (Chen and Wolf 1993; Lyons et al. 2010; Pontius and Wolf 1990). Braking of the earthward flow generates dawnward inertial current, which is supposed to connect to the FACs (Haerendel 1992; Shiokawa et al. 1997a). An auroral streamer is thought to be a projection of this earthward fast flow.

The intense, localized upward FACs associated with the surge have been explained in terms of partial blockage of the ionospheric Hall current (Kan et al. 1984), and a feedback instability (Rothwell et al. 1984, 1988). The surge is also thought to be a projection of an intrusion of the plasma sheet boundary layer into the tail lobe (Akasofu et al. 1971; Bythrow and Potemra 1987).

2.1.4 Recovery phase

The surge slows down and the poleward most aurora attains for 10–30 min (Akasofu 1964). The auroral oval on the nightside sometimes splits into two branches, which are referred to as double oval (Elphinstone et al. 1995b). The poleward branch is caused by accelerated electrons, occasionally accompanied by electrons accelerated by Alfvén waves; whereas the equatorward branch is preferred to be caused by diffusive precipitation of energetic electrons (Ohtani et al. 2012). A north–south aligned auroral structure appears as if it bridges the poleward and the equatorward branches (Henderson et al. 1998; Nakamura et al. 1993; Zesta et al. 2000). Isolated and cloud-like patches, which are also known as pulsating aurora, are present, which drift away from midnight (Akasofu 1964; Opgenoorth et al. 1994; Royrvik and Davis 1977). The intensity of the electrojet recovers gradually.

2.2 Energy transfer

Knowing the electric field and the conductivity, one can calculate the Joule dissipation rate in the ionosphere. The maximum Joule dissipation rate is of the order of $\sim 10^{11}$ W during the expansion phase (Ahn et al. 1983; Kamide et al. 1996; Østgaard 2002; Palmroth et al. 2005; Richmond et al. 1990; Rostoker et al. 1980; Sun et al. 1985; Tanskanen et al. 2002; Zhou et al. 2011). The energy input rate from the solar wind to the magnetosphere has been estimated using the ϵ parameter (Perreault and Akasofu 1978) that is given by

$$\epsilon(W) = \frac{4\pi}{\mu_0} V_{\text{SW}} B_{\text{IMF}}^2 I_0^2 \sin^4 \frac{\theta}{2}, \quad (1)$$

where $I_0 \approx 7 R_E$, V_{SW} is the solar wind speed, B_{IMF} is the magnitude of IMF, θ is angle from the north ($\equiv \tan^{-1} B_y/B_z$), and μ_0 is the magnetic constant. (The original version of the ϵ parameter is provided by the CGS unit. Koskinen and Tanskanen (2002) provided the version in the SI unit, and discussed the meaning of the factor of 4π .) Perreault and Akasofu (1978) considered the Poynting flux in the interplanetary field and an opening area where the Poynting flux enters the magnetosphere.

The kinetic energy of the solar wind is also suggested to participate in the energy supplied into the magnetosphere (Nishida 1983; Vasyliunas et al. 1982).

Traditionally, the energy consumed in the ionosphere during the expansion phase is considered to have two sources. One is associated with a directly driven (DD) process, in which the energy is directly transferred from the solar wind to the ionosphere (Akasofu 1979; Perreault and Akasofu 1978). The other is associated with an unloading (UL) process, in which the energy is stored (in the growth phase) and released (in the expansion phase) in the lobe (Hones 1979; McPherron et al. 1973; McPherron 1970). A linear prediction filtering technique is introduced to investigate the time lag between the solar wind and the auroral electrojet (Bargatze et al. 1985). They found two responses at time lags of 20 min and 60 min. The former lag (20 min) may correspond to the DD process, and the latter one (60 min) may correspond to the UL process. The DD processes are thought to persist through the entire substorm period; whereas the UL processes are dominant when additional FACs are present during the expansion phase (Kamide and Kokubun 1996). The correlation coefficient between the ϵ parameter and the westward electrojet is 0.81 for the substorm expansion phase (Tanskanen et al. 2002). This implies that the amount of the Joule dissipation rate depends on the solar wind energy input regardless of the processes (DD, or UL). Using the ϵ parameter as a proxy of the energy input rate, Baker et al. (1997) comprehensively evaluated the energy budgets from the solar wind to the energy loss. They estimated the energy rate from the solar wind to be 10^{13} – 10^{14} W. The energy loss rates for the ring current injection, ionospheric Joule heating, auroral precipitation, and plasmoid are estimated to be 10^{11} – 10^{12} , 10^{10} – 10^{11} , 10^9 – 10^{10} , and 10^{11} – 10^{12} W, respectively. During the substorm, the energy stored in the magnetotail is estimated to be 10^{15} – 10^{16} J, and the energy dissipation is to be $\sim 3 \times 10^{15}$ J. This means the stored energy is sufficient to supply energy to the ionosphere during the substorm (Baker et al. 1997).

3 Global MHD simulation

3.1 Ability and inability of global MHD simulation

The MHD simulation has intrinsic limitations. First, it cannot deal with kinetic processes. Bright aurora is usually caused by electrons precipitating into the upper atmosphere. The electrons are accelerated by quasi-electrostatic parallel potential, or Alfvén waves. Kinetic treatment is necessary to incorporate the electron acceleration process. The instabilities that are suggested to cause the current disruption in the near-Earth tail region (Lui 1996) cannot be treated correctly. The FACs associated with the Hall current system in the reconnection site are caused by ion–electron decoupling (Nagai et al. 2003). Therefore, one-fluid treatment cannot reproduce the FACs near the reconnection site. The origin of the anomalous resistivity in the reconnection site is problematic. Wave–particle interactions are thought to play an important role in the anomalous resistivity (Fujimoto et al. 2011; Treumann 2001). However, the MHD simulation cannot deal with the wave–particle interaction. Current-aligned instabilities, for instance, lower-hybrid drift instability and ion-acoustic

waves, are also considered to increase the anomalous resistivity (Ricci et al. 2004; Rowland and Palmadesso 1983). Key processes leading to the current disruption and the onset of magnetic reconnection are fundamental for understanding the substorm onset mechanism.

In spite of the inherent limitations, global magnetohydrodynamics (MHD) simulations have shown the features that resemble observed ones during the substorm, such as (1) global evolution of auroral patterns that are similar to sun-aligned arcs, a quiet arc, westward traveling surge (Ebihara and Tanaka 2016; Fedder et al. 1995; Palmroth et al. 2006; Tanaka 2015), (2) localized auroral patterns (Raeder et al. 2012), (3) an intensification of auroral electrojets in the ionosphere (Lopez et al. 2001; Lyon et al. 1998; Raeder et al. 2001; Tanaka et al. 2010; Wiltberger et al. 2000), (3) midlatitude positive bay of ground magnetic disturbance (Tanaka 2015), (4) geomagnetic disturbances from pole to equator including overshielding condition (Ebihara et al. 2014), (5) evolution of the polar cap boundary (Lopez et al. 2001), (6) earthward fast flow and associated enhancement of the magnetic field in the plasma sheet (Birn et al. 2011b; Hesse and Birn 1994; Raeder et al. 2010a; Slinker et al. 2001; Tanaka 2000; Yao et al. 2015a, b), (7) formation of a pair of FACs associated with substorm expansion (Birn et al. 1999; Birn and Hesse 1991; Ebihara and Tanaka 2015a; Tanaka 2015), and (8) formation of multiple near-Earth neutral lines (El-Alaoui et al. 2009).

Our intension here is to overview what the MHD simulation can sufficiently account for the observed auroral transients in the context of a priori presence of anomalous resistivity leading to magnetic reconnection. We believe that verifying the capability of the MHD simulation is useful to identify what is the essential process leading to the observed effects. Of course, we cannot discuss the kinetic processes, and exclude the possibility that current disruption triggers the onset of the substorm expansion.

3.2 Evolution of auroral substorm

Figure 3 shows the evolution of FACs at the ionosphere altitude in the Northern Hemisphere. The FACs are obtained by the global MHD simulation, REPPU (Tanaka, 2015). Readers may refer to Tanaka (2015) for detailed information about the REPPU code. In the REPPU code, the ionosphere is coupled with the magnetosphere by the following means (Tanaka 1994): (1) The FACs, the plasma pressure, and the plasma temperature are mapped from the inner boundary of the simulation domain to the ionosphere altitude. (2) On the basis of these quantities, the ionospheric conductivity (Hall and Pedersen conductivities) is calculated. The detailed calculation of the conductivity is given by Ebihara et al. (2014). (3) For given FACs and the conductivity, the ionospheric electric potential is calculated by solving an ellipse partial differential equation. (4) The calculated electric field is mapped from the ionospheric altitude to the inner boundary of the simulation domain. The above cycle is repeated every ~ 0.02 s. We believe that the mutual coupling between

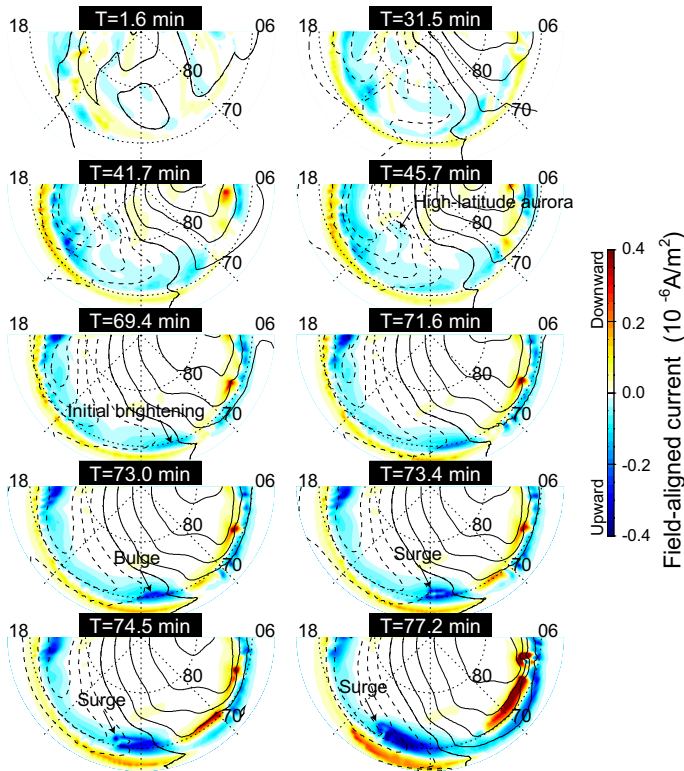


Fig. 3 Evolution of field-aligned currents (negative upward) at the ionosphere altitude (After Ebihara and Tanaka 2016). The contour line indicates the ionospheric electric potential at an interval of 5 kV. The solid and dashed lines indicate the positive and negative potentials, respectively. The Sun is towards the top. The lower boundary is located at 65 magnetic latitudes (MLATs)

the magnetosphere and the ionosphere is reasonably achieved as a zeroth order approximation.

To obtain a quasi-steady magnetosphere, a northward IMF condition was initially imposed to the simulation for the first 2 h of the simulation with the following parameters: a solar wind density of 5.0 cm^{-3} , a solar wind speed of 372 km s^{-1} , the Y -component of the interplanetary magnetic field (IMF B) at -2.5 nT , and the IMF B_z at 4.3 nT . IMF B_x was held at 0 throughout the calculation. IMF B_z was changed to -3.0 nT after 2 h. The epoch time “ $T=0$ ” is referred to as the moment when the southward IMF reached $X=40 \text{ Re}$. The detailed setting and parameters of this particular simulation are described by Ebihara and Tanaka (2016).

Figure 4 summarizes the calculated Auroral Upper (AU) and Auroral Lower (AL) indices (Davis and Sugiura 1966), and the FACs as a function of the magnetic latitude (MLAT) and time at the meridian of 0.8 h magnetic local time (MLT). The AU and AL indices were obtained by the following means (Ebihara and Tanaka 2015b). The H-component (north–south component) of the magnetic disturbance on

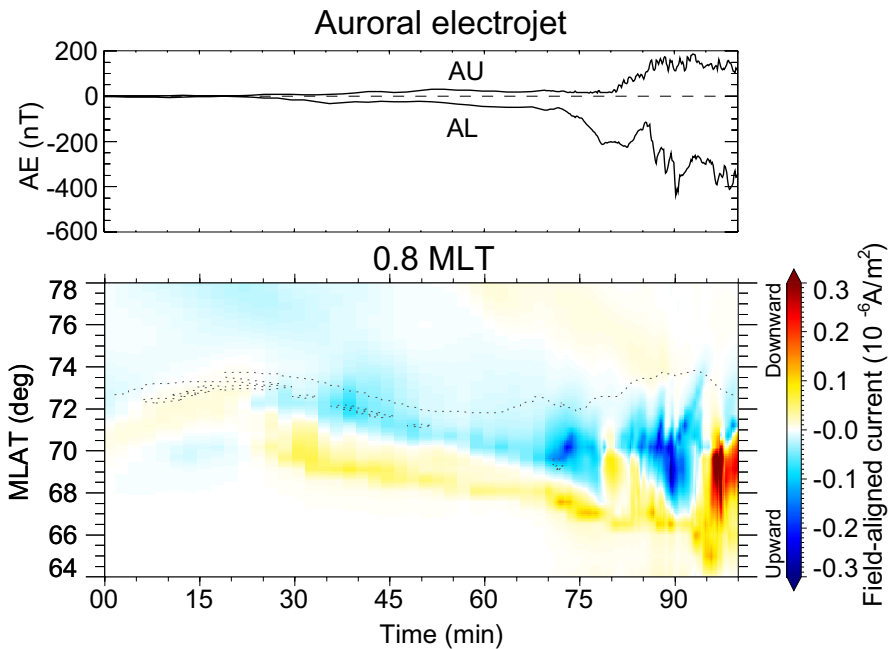


Fig. 4 (top) Auroral electrojet indices, AU and AL, and (bottom) field-aligned current at the ionosphere altitude as a function of the magnetic latitude (MLAT) and time at the meridian of 0.8 h magnetic local time (MLT). The dashed line in the bottom panel indicates the boundary between the open and closed field lines

the ground at 48 MLTs with an interval of 0.5 h at 70 MLAT was calculated. The magnetic disturbances were calculated based on the Hall current flowing in the ionosphere. After superposing the magnetic disturbances, we regard the upper envelope of the magnetic disturbance as AU, and the lower one as AL.

Simultaneous optical and particle observations have shown that bright aurora is caused by the precipitating electrons accelerated by electric field parallel to the magnetic field line (Fujii et al. 1994; Weimer et al. 1994). Quasi-electrostatic upward electric field is observed in the upward FAC region (Elphic et al. 1998; Lyons et al. 1979; Sakanoi et al. 1995; Weimer et al. 1987). It may be reasonable to consider that the upward FAC is a proxy of the bright aurora in that sense. The following is a brief summary of the evolution of auroral substorm reproduced by the REPPU code. Hereinafter, we refer to the upward FAC as aurora for the sake of simplicity.

3.2.1 Northward IMF ($T=1.6$ min)

In Fig. 3, some elongated auroral structures (upward FACs) are found at high latitudes. They resemble the sun-aligned arcs that are often observed for northward IMF (Davis 1962; Eliasson et al. 1987; Frank et al. 1982; Ismail et al. 1977; Lassen and Danielsen 1978; Meng and Lundin 1986; Newell et al. 1997; Shiokawa et al. 1995, 1997b). According to the REPPU code, the auroral structures are closely associated

with the flow vorticity near protuberances of high-pressure region (Ebihara and Tanaka 2016). The protuberances are developed in the northward IMF condition due to interchange-like instability resulting from the magnetosphere–ionosphere coupling.

3.2.2 Growth phase ($T=31.5, 41.7$ and 45.7 min)

At a glance, two types of large-scale FACs, called Region 1 and Region 2 FACs (Iijima and Potemra 1976), are clearly found in Fig. 3. The Region 1 FAC is a pair of the FACs (flowing into the ionosphere on the dawnside, and away from it on the duskside). The Region 2 FAC is located equatorward of the Region 1 FAC. The polarity of the Region 2 is opposite to that of the Region 1 FAC.

The auroral structures, which resemble the sun-aligned arcs during the northward IMF condition, move equatorward. We call them high-latitude aurorae for the sake of simplicity. In the course of the equatorward movement, the direction of the high-latitude aurora changes from east–west to north–south, and vice versa. This is consistent with the observation (Nishimura et al. 2010a). The equatorward movement of the high-latitude aurora is a manifestation of the movement of the protuberance from the high-latitude magnetosphere to the low-latitude magnetosphere (Ebihara and Tanaka 2016). The equatorward movement of the protuberance is caused by the development of the magnetospheric convection under the southward IMF. The development of the convection electric field is also seen in the ionosphere as shown in Fig. 3.

The auroral structure that resembles the quiet arc, which is elongated to the east and west directions, has also been presented by global MHD simulations (Fedder et al. 1995; Palmroth et al. 2006; Ream et al. 2013; Tanaka 2015; Wiltberger et al. 2009). According to the REPPU code, the quiet auroral arc is closely associated with flow shear in the Y -direction of the high-latitude magnetosphere. The convection flow originating from the higher latitude is deflected toward the dawn and dusk directions (Tanaka 2015). Both the high-latitude auroras and the quiet arc are not necessarily a projection of the magnetospheric processes taking place in the equatorial plane.

Figure 4 shows that the AL index gradually decreases and the quiet arc moves equatorward. These gradual transients are consistent with the observations (Fukunishi 1975; Kadokura et al. 2002; McPherron 1970).

3.2.3 Early stage of expansion phase ($T=69.4, 71.6$ and 73.0 min)

Figure 3 shows that the bright aurora longitudinally elongated appears first (at $T=69.4$ and 71.6 min), followed by a bulge-like one (at $T=73.0$ min). The bright aurora starts to appear near the equatorward border of the preexisting auroral arc (as indicated by upward FAC region) as shown in Fig. 4. These are consistent with the observations (Akasofu 1964). The small-scale auroral structures, beads, or optical wave-like structures (Henderson 2009; Liang et al. 2007; Rae et al. 2010; Sakaguchi et al. 2009), are not clearly identified in the simulation result of the REPPU code. Small-scale FACs that are not resolved by the current version of the REPPU code,

or kinetic processes that are non-MHD ones may be involved for the generation of such small-scale structures.

Because of an increase in the anomalous resistivity that is a function of the magnetic field and the current density (Tanaka et al. 2010), a NENL appears first, in this particular run, at $\sim 40 R_E$ downtail of the Earth at $T \sim 56$ min (Ebihara and Tanaka 2016). The location of the NENL is fairly tailward of that typically observed (Angelopoulos et al. 1994; Baker et al. 1996; Machida et al. 2009; Nagai et al. 1998; Nishida and Nagayama 1973). The simulation result of the REPPU code with different solar wind parameter shows that the NENL appears at $\sim 17 R_E$ downtail (Tanaka et al. 2017). The location of the NENL is still under investigation. The formation of the NENL results in the earthward and tailward fast flows in the plasma sheet. The earthward fast flows (BBFs) are well reproduced by global MHD simulations (Birn et al. 2011b; Hesse and Birn 1994; Raeder et al. 2010b; Slinker et al. 2001; Tanaka 2000). Multiple NENLs can also form (El-Alaoui et al. 2009).

Figure 5 shows a schematic illustration of typical paths of earthward plasma flow found in the global MHD simulation during the expansion phase (e.g., Ebihara and Tanaka 2017). The BBF belongs to the equatorial path shown by the blue line. As the earthward flow approaches the Earth, the flow splits into two, one directing toward dawn, and the other toward dusk. The flow shears (vorticities) associated with the split of the flow give rise to the generation of FACs (Birn et al. 1999; Birn and Hesse 1991, 2014). This is consistent with observations (Keiling et al. 2009), and is thought to form the current wedge that connects the equatorial plane and the ionosphere. The paths and the location of the shear (vorticity) are illustrated in Fig. 6.

The result of the global MHD simulation, however, shows that the FACs generated in the equatorial plane cannot form a current wedge completely (connecting to the ionosphere). The reason is that the plasma pressure significantly increases near the equatorial plane due to compression of the plasma. The increase in the plasma pressure is inevitable during the dipolarization. As a consequence of the increase in the plasma pressure, the diamagnetic current (flowing perpendicular to the magnetic field) develops, which can overcome the FACs. The current lines are no longer field-aligned, and are not connected to the ionosphere as drawn in Fig. 6 (Ebihara and Tanaka 2015a). The significant increase in the plasma pressure has been observed by the THEMIS satellite (Yao et al. 2015a, b). One may consider that the shear

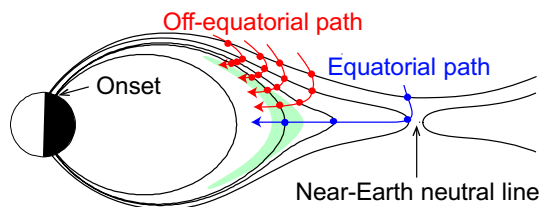


Fig. 5 Paths of earthward plasma flow in the meridional plane during the expansion phase (Ebihara 2019). The greenish area represents the region where the plasma pressure is high. The high-pressure region is essentially caused by compression of plasma (rather than advection)

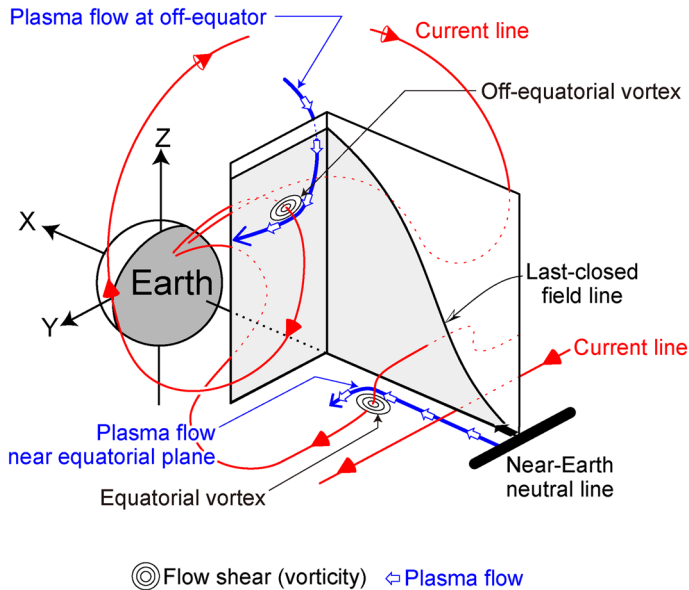


Fig. 6 Paths of plasma (blue line) and current lines (red lines) during the expansion phase (Ebihara 2019). The shaded area represents the region of closed field lines

generated in the equatorial plane propagates toward the Earth along a field line as an Alfvén wave, so as to carry the FACs. To propagate the Alfvén wave along a field line, the FAC must be coupled with the inertial current. The presence of the diamagnetic current will impede the field-aligned propagation of the FAC near the equatorial plane, in particular, during the expansion phase.

According to the global MHD simulations, the off-equatorial path, which is schematically drawn by the red lines in Fig. 5, participates more directly in the generation of the FACs associated with the expansion onset (Birn and Hesse 2005; Ebihara and Tanaka 2015a). The plasma originating in the lobe traverses the open–closed boundary (separatrix). After traversing the separatrix, the plasma travels toward the equatorial plane until the pressure gradient force becomes significant. Finally, the plasma flow splits into two, one directing toward the dawn, and the other toward the dusk. The dawnward and the duskward flows generate two pairs of FACs. (Ebihara and Tanaka 2015a, 2017). At high-latitude magnetosphere (and relatively low altitude), the plasma beta is low, and the diamagnetic current is relatively small. The total current (which is a sum of the perpendicular and parallel currents) is closely aligned with the field line (c.f., Figure 8g of Ebihara and Tanaka 2015a). When the FACs arrive at the ionosphere, the expansion phase of the auroral substorm begins.

Birn and Hesse (2013) pointed out that the FACs associated with the expansion onset are located well equatorward of the boundary between the open and closed magnetic field lines. Figure 4 shows that the open–closed boundary is located at $\sim 72^\circ\text{--}73^\circ$ MLAT at the expansion onset. The brightening of the aurora, however, starts to appear at $\sim 69.7^\circ$ MLAT, which is located near the equatorward

border of the preexisting auroral arc, rather than the open–closed boundary. This implies that the NENL model does not always predict the onset location to be near the open–closed boundary. The NENL model can reasonably account for the observational fact that the auroral brightening starts near the equatorward border of the preexisting auroral arc. The reason is that the plasma can traverse the separatrix, and penetrate deep into the inner region until the pressure force (both the magnetic force and the plasma pressure force) impedes the inward penetration as schematically drawn in Fig. 6.

The global MHD simulations have reproduced an abrupt development of the westward electrojet as manifested by the sudden decrease in the AL index (Fedder et al. 1995; Lyon et al. 1998; Raeder et al. 2001; Wiltberger et al. 2000). Figure 4 shows that the AL index starts decreasing abruptly at $T \sim 70$ min.

3.2.4 Later stage of expansion phase ($T = 73.4, 74.5$ and 77.2 min)

A surge-like structure appears at the latter stage of expansion phase in the simulation result shown in Fig. 3. The surge tends to travel westward, which resembles the WTS (Akasofu 1964). In the simulation, the WTS appears as a consequence of the ionosphere–magnetosphere coupling. The possible explanation can be summarized as follows (Ebihara and Tanaka 2015b, 2018): (1) The conductivity increases first in a part of the ionosphere at the early stage of the expansion phase. (2) The ionospheric Hall current ($= \Sigma_H \mathbf{B} \times \mathbf{E}/B$, where Σ_H is the Hall conductivity) overflows near the poleward, or westward edge of the high-conductivity region. (3) To conserve the current continuity, the Hall current must be connected to the Pedersen current and the FACs. Most of the remnant Hall current (about 90%) is connected to the FACs, and the rest of it (about 10%) is connected to the Pedersen current ($= \Sigma_p \mathbf{E}$, where Σ_p is the Pedersen conductivity). The Pedersen current related to the upward FAC is divergent, that is, $\nabla \cdot \mathbf{E} > 0$. Figure 7 shows a close-up view of the FACs at $T = 74.5$ min. The yellow contour indicates the region where $\nabla \cdot \mathbf{E} > 0$. (4) When the divergent electric field propagates to the magnetosphere, it gives rise to flow shear (vorticity) of plasma. (5) Upward FAC is further intensified by the locally generated flow shear (vorticity). (6) Bright aurora appears just poleward, or just westward of the high-conductivity region. The ionospheric conductivity increases in accordance

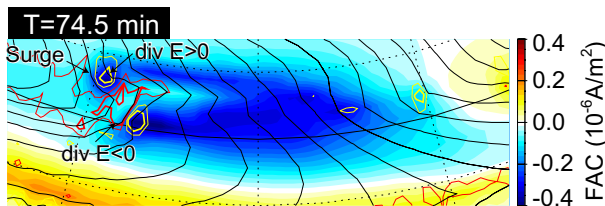


Fig. 7 Structured upward field-aligned currents during the substorm expansion phase, which manifest the westward traveling surge of bright aurora. The yellow contour indicates the region where $\nabla \cdot \mathbf{E} > 0$, whereas the red one indicates the region where $\nabla \cdot \mathbf{E} < 0$. The black contour indicates the equipotential of the electric field (Ebihara and Tanaka 2018)

with the bright aurora. (7) The opposite processes take place. Namely, the ionospheric Hall current lacks near the equatorward, or eastward edge of the high-conductivity region. Convergent electric field ($\nabla \cdot \mathbf{E} < 0$) appears, giving rise to the flow shear (vorticity) that reduces the upward FAC. The red contour in Fig. 7 indicates the region where $\nabla \cdot \mathbf{E} < 0$. (8) By repeating the cycle from (2) to (7), the surge travels in the direction of the Hall current, namely poleward, or westward. This process is similar to the partial blockage model (Kan et al. 1984).

The traveling surge structure appears only in the upward FAC, whereas it is absent in the downward FAC. This asymmetry comes from the simulation setting that the ionospheric conductivity increases in the region where the upward FAC flows (as a proxy of discrete aurora) and/or the plasma pressure is high (as a proxy of diffuse aurora). Ebihara and Tanaka (2018) performed a numerical experiment in which the ionospheric conductivity increases regardless of the polarity of the FAC. The result shows that an eastward traveling surge appears in the downward FAC region. This experiment explains the reason why the surge travels primarily westward, and suggests that the surge is a manifestation of the magnetosphere–ionosphere coupling, not a projection of the magnetospheric structure. Of course, the MHD simulation cannot deal with the kinetic processes that are supposed to participate in the formation of surge and the magnetosphere–ionosphere coupling. The role of the kinetic process in the formation of the surge remains unsolved.

For the large-scale FACs, both the Region 1 and Region 2 FACs are found to increase simultaneously, in particular, on the nightside. This is consistent with the observations (Anderson et al. 2014; Coxon et al. 2014). The development of these FACs can be understood to the two pairs of shears (vorticities) at off-equator (shown in Figure 10 of Ebihara and Tanaka, 2017). The shears are closely associated with the off-equatorial paths shown in Fig. 5. According to the global MHD simulation, the Region 2 FAC that increases during the expansion phase is connected to the incomplete current wedge near the equatorial plane as shown in Fig. 6. This is different from the previous thought that the Region 1-sense FAC associated with the substorm is connected to the current wedge.

The small-scale auroral structures, which are presumably related to electrons accelerated by Alfvén waves, are often observed poleward of the surge (Mende et al. 2011; Weimer et al. 1994). These auroral structures cannot be identified in the global MHD simulation result. Simultaneous particle and optical observations have shown that the Alfvénic aurora is associated with electrons accelerated by inertial Alfvén waves under the presence of strong flow shear (Asamura et al. 2009). The generation mechanism of the inertial Alfvén waves and its relationship to the large-scale processes are subjects of future research.

3.3 Energy transfer and conversion

3 types of energy can be defined in the MHD approximation (Birn and Hesse 2005; Cravens 1997). The first type of energy is the internal energy density u . For an ideal monatomic gas, the ratio of specific heats γ is 5/3. For the isotropic gas, the internal

energy density u yields $3P/2$, where P is the plasma pressure. The equation for the transport of the internal energy density is given by

$$\frac{\partial u}{\partial t} + \nabla \cdot (\gamma u \mathbf{V}) = \mathbf{V} \cdot \nabla P, \tag{2}$$

where \mathbf{V} is the plasma bulk velocity. Because of γ on the left-hand side, Eq. (2) does not directly represent the continuity of u . We focus only on the right-hand side of Eq. (2) that governs the energy conversion. The second type is the bulk kinetic energy density ($=\rho v^2/2$), where ρ is the mass density. The equation for the transport of the kinetic energy density is given by

$$\frac{\partial}{\partial t} \left(\frac{\rho}{2} v^2 \right) + \nabla \cdot \left(\frac{\rho}{2} v^2 \mathbf{V} \right) = \rho \mathbf{V} \cdot \frac{d\mathbf{V}}{dt} = \mathbf{V} \cdot (\mathbf{J} \times \mathbf{B} - \nabla P), \tag{3}$$

where \mathbf{B} and \mathbf{J} are the magnetic field, and the current density, respectively. The third type is the potential energy. Neglecting the gravitational force, the potential energy includes the magnetic energy density ($=B^2/2\mu_0$) and the electric energy density ($=\epsilon_0 E^2/2$), where E , μ_0 and ϵ_0 are the electric field, the magnetic constant and the electric constant, respectively. In the MHD approximation, the electric energy density can be neglected because of the absence of the displacement current. With the aid of Poynting’s theorem, the equation for the transport of the magnetic energy is given by

$$\frac{\partial}{\partial t} \left(\frac{B^2}{2\mu_0} \right) + \nabla \cdot \mathbf{S} = -\mathbf{J} \cdot \mathbf{E} = -\mathbf{V} \cdot (\mathbf{J} \times \mathbf{B}), \tag{4}$$

where \mathbf{S} is the Poynting flux given by

$$\mathbf{S} = \frac{\mathbf{E} \times \mathbf{B}}{\mu_0}. \tag{5}$$

The resistivity is assumed to be zero for the derivation of the last term of Eq. (4). The last term of Eq. (4) implies the opposite of the work done by the Lorentz force on the bulk flow \mathbf{V} . Here, we simply define a dynamo region as that where $\mathbf{J} \cdot \mathbf{E} < 0$.

Figure 8 shows a perspective view of a main path of the magnetic energy obtained by the global MHD simulation, REPPU (Ebihara et al. 2019). The interplanetary magnetic field (IMF) is southward and the substorm expansion has just begun. Magnetic reconnection is ongoing in the two sites this moment. One is in the dayside magnetopause and the other is in the near-Earth plasma sheet. The white line indicates an integral curve of the Poynting flux \mathbf{S} , which is referred to as an S -curve (Ebihara and Tanaka, 2017). The following equation is solved to draw the S -curve,

$$\mathbf{R}(L) = \mathbf{R}(0) + \int_0^L \left(\frac{\mathbf{S}(\mathbf{R}(l))}{S} \right) dl, \tag{6}$$

where l is the distance from an arbitrary starting point, \mathbf{R} is the position vector. The S -curve coming from the solar wind (left) shows a spiral with its center moving

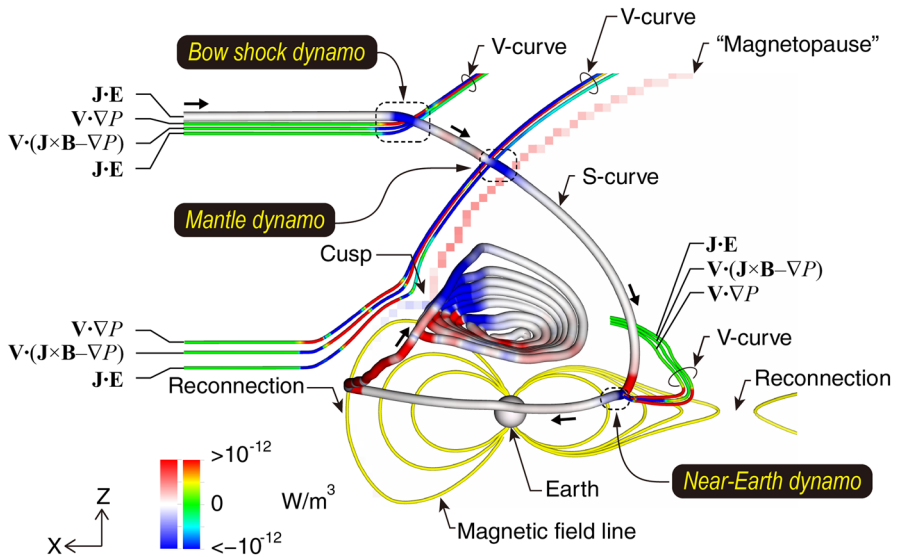


Fig. 8 Main path of magnetic energy from solar wind to ionosphere at the onset of the auroral substorm expansion. The whitish line indicates an integral curve of the Poynting flux (*S*-curve), and the greenish lines indicate integral curves of the plasma bulk velocity (*V*-curve). The yellow lines indicate the magnetic field lines. The Sun is to the left (After Ebihara et al. 2019)

toward the Earth (white sphere). Since the inner boundary of the global MHD simulation is located at 2.6 earth-radii (R_E), the *S*-curve is not drawn in the low-altitude region of the magnetosphere. In the low-altitude magnetosphere, a large amount of the magnetic energy is probably transferred to the kinetic energy of electrons precipitating into the ionosphere (Lu et al. 1998; Palmroth et al. 2004). The color code on the *S*-curve represents the value of $\mathbf{J} \cdot \mathbf{E}$, indicating that there are a few dynamo regions where $\mathbf{J} \cdot \mathbf{E} < 0$, near the bow shock, in the mantle (near the high-latitude magnetopause), and in the near-Earth region on the nightside. Three green lines indicate integral curves of the plasma bulk velocity, namely, stream lines of plasma (*V*-curve). The color codes on the greenish lines indicate the values of the right-hand sides of Eq. (2), (3), and (4). There is another dynamo region poleward of the cusp. As the *S*-curve traverses the cusp from the equatorward part to the poleward part, the magnetic energy is converted into the kinetic energy ($\mathbf{J} \cdot \mathbf{E} > 0$ as indicated by red color), followed by the internal energy, the kinetic energy, and the magnetic energy ($\mathbf{J} \cdot \mathbf{E} < 0$ as indicated by blue color). Thus, the energy conversion is almost completed near the cusp. We do not mention the ‘cusp’ dynamo here because the contribution to the auroral substorm is unknown.

3.3.1 Bow shock dynamo

Obviously, $\mathbf{V} \cdot (\mathbf{J} \times \mathbf{B} - \nabla P) < 0$, $\mathbf{V} \cdot \nabla P > 0$, and $\mathbf{J} \cdot \mathbf{E} < 0$ near the bow shock. This implies that a part of the solar wind kinetic energy is converted into the internal energy and the magnetic energy. The magnetic energy generated through

compression in the bow shock is suggested to be consumed in the dayside reconnection region (Siebert and Siscoe 2002). The MHD simulation results show that some currents passing through the bow shock close in the ionosphere, known as the Region 1 FAC (Fedder et al. 1997; Guo et al. 2008; Siscoe and Siebert 2006). The bow shock dynamo appears regardless of the polarity of the IMF (Tanaka 1995), whereas the magnitude of the Region 1 FAC increases with the southward component of IMF (SBZ) (Anderson et al. 2008; Weimer 2005). This implies that the existence of the bow shock dynamo does not solely explain the Region 1 FAC. Recently, the bow shock dynamo is confirmed to exist, and the main region of the current closure is located further tailward (Hamrin et al. 2018).

3.3.2 Mantle dynamo

The mantle dynamo appears when IMF is southward (Tanaka 1995). In the mantle dynamo, $\mathbf{V} \cdot (\mathbf{J} \times \mathbf{B} - \nabla P) > 0$, $\mathbf{V} \cdot \nabla P < 0$, and $\mathbf{J} \cdot \mathbf{E} < 0$, implying that the internal energy is converted into the kinetic energy and the magnetic energy. As previously pointed out by Tanaka et al. (2016), the simulation result is different from the previous view in which the solar wind (magnetosheath) kinetic energy is decreased, and the kinetic energy is directly converted into the magnetic energy due to tangential stress against the solar wind motion (Akasofu 1974; Siscoe and Cummings 1969). The momentum flux from the solar wind (magnetosheath) motion to the magnetosphere is also discussed by Wright (1996). The MHD simulation results show that the solar wind (magnetosheath flow) kinetic energy is not decreased, but increased (Tanaka 2007). The increase in the kinetic energy is sustained by the release of the internal energy. Interestingly, $\nabla \cdot \mathbf{V}_\perp < 0$, whereas $\nabla \cdot \mathbf{V}_\parallel > 0$, implying that the field-perpendicular flow decreases; whereas the field-aligned flow increases in moving frame of reference. This configuration is referred to as an expansion slow dynamo. The condition that $\nabla \cdot \mathbf{V}_\perp < 0$ may be related to the energy conversion into the magnetic energy (Watanabe et al. 2019).

The immediate origin of the internal energy can be found in the equatorward part of the (exterior) cusp by tracing the V -curve backward from the mantle dynamo. In the equatorward part of the cusp, $\mathbf{V} \cdot (\mathbf{J} \times \mathbf{B} - \nabla P) < 0$, $\mathbf{V} \cdot \nabla P > 0$, and $\mathbf{J} \cdot \mathbf{E} > 0$, implying that the kinetic and the magnetic energies are converted into the internal energy. This conversion process is described by Tanaka (2007) in detail.

3.3.3 Near-Earth dynamo

In the global MHD simulation, the near-Earth dynamo appears as a consequence of the formation of the magnetic reconnection taking place in the near-Earth tail region. In the near-Earth dynamo, $\mathbf{V} \cdot (\mathbf{J} \times \mathbf{B} - \nabla P) > 0$, $\mathbf{V} \cdot \nabla P < 0$, and $\mathbf{J} \cdot \mathbf{E} < 0$, implying that the internal energy is converted into the kinetic energy and the magnetic energy. The internal energy plays an important role in the near-Earth dynamo and in the generation of the FACs associated with the substorm expansion (Birn and Hesse 2005; Ebihara and Tanaka 2015a, 2017). The process for the increase in the internal energy depends on the paths, the equatorial path, or the off-equatorial path.

The equatorial path (indicated by the blue line in Fig. 5) comes from the lobe region by way of the near-Earth reconnection site. When a plasma parcel passes through the reconnection region, the magnetic energy splits into the kinetic energy and the internal energy (Birn et al. 2010, 2011a). The plasma parcel moving earthward near the equatorial plane is called a bursty bulk flow (BBF) (Angelopoulos et al. 1992; Baumjohann et al. 1990). The earthward plasma parcel is decelerated when it approaches the region where the magnetic and plasma pressure is high. This is called flow braking. Consequently, the plasma pressure increases due to compression. The kinetic energy is converted into the internal energy, followed by the magnetic energy. Observations made by the Cluster satellites have shown the presence of this conversion near the equatorial plane (Hamrin et al. 2014). The earthward flow splits into the duskward and downward flows (Birn et al. 2004, 2011b; Birn and Hesse 1991), giving rise to a flow shear. The flow shear is thought to generate Region 1-sense FACs that give rise to the expansion onset (Keiling et al. 2009; Yao et al. 2012). This idea is based on the assumption that the FACs generated in the equatorial plane are transferred to the ionosphere without significant damping. According to the global MHD simulation, the diamagnetic current is significantly enhanced near the equatorial plane because of the enhancement of the plasma pressure (Ebihara and Tanaka 2015a). Due to the presence of the diamagnetic current, the Alfvén waves cannot travel toward the ionosphere efficiently, and the current line is no longer field-aligned (Ebihara and Tanaka 2015a; Tanaka et al. 2010, 2017) as mentioned above.

For the off-equatorial path (indicated by the red line in Fig. 5), a plasma parcel traverses the separatrix of the newly reconnected field line; energy conversion from the magnetic energy to the internal energy takes place well equatorward of the separatrix (where $\mathbf{V} \cdot \nabla P > 0$, and $\mathbf{J} \cdot \mathbf{E} > 0$). The kinetic energy is not significantly involved for the increase in the internal energy. The FACs that are closely associated with the substorm expansion are generated at off-equator where the diamagnetic current is relatively small (Birn and Hesse 2005; Ebihara and Tanaka 2015a, 2017). The existence of the off-equatorial near-Earth dynamo has been confirmed by the Cluster satellite observations (Marghitu et al. 2006).

3.3.4 Low-altitude dynamo

The ionospheric Hall current overflows (and lacks) when the ionospheric conductivity is inhomogeneous (Kan et al. 1984). When the Hall current is not perfectly connected to the FACs, space charge (as represented by the condition that $\nabla \cdot \mathbf{E} \neq 0$) arises. When the electric field propagates to the magnetosphere, a flow shear (vorticity) appears, giving rise to the work done on the Lorentz force (and generation of the additional FACs). Figure 9 shows the $\mathbf{J} \cdot \mathbf{E}$ value on the sphere at the geocentric distance of $3.2 R_E$. Negative $\mathbf{J} \cdot \mathbf{E}$ is clearly found above the leading ($\nabla \cdot \mathbf{E} > 0$) edge of the surge. These results imply that an additional dynamo appears in the low-altitude magnetosphere in association with the space charge deposited by the overflow and lack of the ionospheric Hall current.

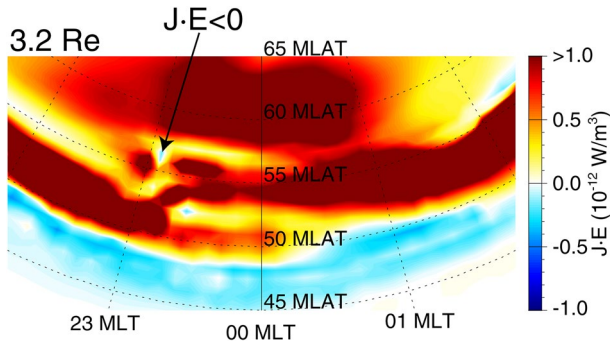


Fig. 9 $J \cdot E$ on the sphere at geocentric distance at $3.2 R_E$ in the magnetosphere at $T = 74.5$ min (Ebihara and Tanaka 2018). MLAT and MLT stand for the magnetic latitude and the magnetic local time, respectively

4 Summary

The global MHD simulation can reproduce some auroral transients evolving from the northward IMF condition to the expansion phase of an auroral substorm. The following processes are found to occur in the MHD simulation.

1. When interplanetary magnetic field (IMF) is northward, complicated auroral structures, including sun-aligned arcs, are found to appear in the MHD simulation. Some auroral structures in the northward IMF are attributed to the flow shear (vorticity) near the protuberance of high-pressure region at high latitudes. The protuberances develop due to interchange-like instability.
2. When the IMF turns southward, the high-latitude aurora is found to move equatorward in the MHD simulation because the protuberance of the high-pressure region moves toward the equatorial plane under the enhanced magnetospheric convection. The quiet arc also appears due to flow shear at off-equator.
3. When a near-Earth neutral line forms in the plasma sheet, bursty bulk flows appear, giving rise to the flow shear (vorticity) near the equatorial plane. The flow shear (vorticity) generates the FACs that resemble a current wedge. Because of the dominance of the diamagnetic current, the current wedge is incomplete, and cannot be connected to the ionosphere. The flow shear (vorticity) generated at off-equator participates more directly in the generation of the FACs associated with the auroral substorm expansion. When the FACs arrive at the ionosphere, the auroral substorm expansion begins.
4. When the aurora becomes bright, the conductivity is higher than ambient. The ionospheric Hall current overflows (lacks) near the edges of the bright aurora, giving rise to an increase (a decrease) in the upward FACs. By repeating this magnetosphere–ionosphere coupling process, a bright aurora (surge) travels in the direction of the Hall current, namely westward in most cases.

It is suggested from the global MHD simulation results that the evolution of the auroral substorm is associated with the evolution of dynamo regions, the bow shock dynamo (which appears when the solar wind is supersonic), the mantle dynamo (which appears when IMF is southward), the near-Earth dynamo (which appears when the near-Earth neutral line forms), and the low-altitude dynamo (which appears when the ionospheric Hall conductivity is not uniform.)

We have to emphasize that the MHD simulation cannot reproduce all the features associated with the auroral substorm, like small-scale auroral structures (beads and wave-like structures) and pulsating aurorae. Further studies are required to investigate the role of kinetic processes and their relationships to the MHD-scale processes.

Acknowledgements The authors thank Professor Emeritus Atsuhiko Nishida and Professor Emeritus Takashi Kikuchi for their insightful and fruitful comments and discussion. The computer simulation was performed on the KDK computer system at the Research Institute for Sustainable Humanosphere (RISH), Kyoto University. This study was supported by JSPS KAKENHI grants 15H03732 and 15H05815, as well as Flagship Collaborative Research and Research Mission 3 “Sustainable Space Environments for Humankind” at RISH, Kyoto University.

Funding This work was supported by JSPS KAKENHI Grant Number 15H03732 and 15H05815, as well as Flagship Collaborative Research and Research Mission 3 “Sustainable Space Environments for Humankind” at RISH, Kyoto University.

Compliance with ethical standards

Conflicts of interest The authors declare that they have no conflicts of interest.

Open Access This article is licensed under a Creative Commons Attribution 4.0 International License, which permits use, sharing, adaptation, distribution and reproduction in any medium or format, as long as you give appropriate credit to the original author(s) and the source, provide a link to the Creative Commons licence, and indicate if changes were made. The images or other third party material in this article are included in the article’s Creative Commons licence, unless indicated otherwise in a credit line to the material. If material is not included in the article’s Creative Commons licence and your intended use is not permitted by statutory regulation or exceeds the permitted use, you will need to obtain permission directly from the copyright holder. To view a copy of this licence, visit <http://creativecommons.org/licenses/by/4.0/>.

References

- B.-H. Ahn, S.-I. Akasofu, Y. Kamide, *J. Geophys. Res.* **88**, 6275 (1983). <https://doi.org/10.1029/JA088iA08p06275>
- S.-I. Akasofu, *Planet. Sp. Sci.* **12**, 273–282 (1964). [https://doi.org/10.1016/0032-0633\(64\)90151-5](https://doi.org/10.1016/0032-0633(64)90151-5)
- S.-I. Akasofu, *Space Sci. Rev.* **4**, 498–540 (1965). <https://doi.org/10.1007/BF00177092>
- S.-I. Akasofu, *Planet. Sp. Sci.* **27**, 425–431 (1979). [https://doi.org/10.1016/0032-0633\(79\)90119-3](https://doi.org/10.1016/0032-0633(79)90119-3)
- S.-I. Akasofu, E.W. Hones, M.D. Montgomery, S.J. Bame, S. Singer, *J. Geophys. Res.* **76**, 5985–6003 (1971). <https://doi.org/10.1029/JA076i025p05985>
- S. Akasofu, *J. Geophys. Res.* **68**, 1667–1673 (1963). <https://doi.org/10.1029/JZ068i006p01667>
- S.I. Akasofu, *Planet. Sp. Sci.* **22**, 885–923 (1974). [https://doi.org/10.1016/0032-0633\(74\)90161-5](https://doi.org/10.1016/0032-0633(74)90161-5)
- B.J. Anderson, H. Korth, C.L. Waters, D.L. Green, V.G. Merkin, R.J. Barnes, L.P. Dyrud, *Geophys. Res. Lett.* **41**, 3017–3025 (2014). <https://doi.org/10.1002/2014GL059941>

- B.J. Anderson, H. Korth, C.L. Waters, D.L. Green, P. Stauning, *Ann. Geophys.* **26**, 671–687 (2008). <https://doi.org/10.5194/angeo-26-671-2008>
- V. Angelopoulos, W. Baumjohann, C.F. Kennel, F.V. Coroniti, M.G. Kivelson, R. Pellat, R.J. Walker, H. Lühr, G. Paschmann, *J. Geophys. Res.* **97**, 4027 (1992). <https://doi.org/10.1029/91ja02701>
- V. Angelopoulos, C.F. Kennel, F.V. Coroniti, R. Pellat, M.G. Kivelson, R.J. Walker, C.T. Russell, W. Baumjohann, W.C. Feldman, J.T. Gosling, *J. Geomagn. Geoelectr.* **99**, 21257 (1994)
- V. Angelopoulos, J.P. Mcfadden, D. Larson, C.W. Carlson, S.B. Mende, H. Frey, T. Phan, D.G. Sibeck, K. Glassmeier, U. Auster, E. Donovan, I.R. Mann, I.J. Rae, C.T. Russell, A. Runov, X. Zhou, L. Kepko, *Science* **931**, 931–936 (2008). <https://doi.org/10.1126/science.1160495>
- C.D. Anger, A.T.Y. Lui, S.-I. Akasofu, *J. Geophys. Res.* **78**, 3020–3026 (1973). <https://doi.org/10.1029/JA078i016p03020>
- E.E. Antonova, *Adv. Sp. Res.* **13**, 261–264 (1993). [https://doi.org/10.1016/0273-1177\(93\)90343-A](https://doi.org/10.1016/0273-1177(93)90343-A)
- K. Asamura, C.C. Chaston, Y. Itoh, M. Fujimoto, T. Sakanoi, Y. Ebihara, A. Yamazaki, M. Hirahara, K. Seki, Y. Kasaba, M. Okada, *Geophys. Res. Lett.* **36**, 1–5 (2009). <https://doi.org/10.1029/2008GL036803>
- G. Atkinson, *J. Geophys. Res.* **72**, 5373–5382 (1967). <https://doi.org/10.1029/JZ072i021p05373>
- D.N. Baker, T.I. Pulkkinen, V. Angelopoulos, W. Baumjohann, R.L. McPherron, *J. Geophys. Res. Sp. Phys.* **101**, 12975–13010 (1996). <https://doi.org/10.1029/95JA03753>
- D.N. Baker, T.I. Pulkkinen, M. Hesse, R.L. McPherron, *J. Geophys. Res. Sp. Phys.* **102**, 7159–7168 (1997). <https://doi.org/10.1029/96JA03961>
- D.N. Baker, T.I. Pulkkinen, R.L. McPherron, J.D. Craven, L.A. Frank, R.D. Elphinstone, J.S. Murphree, J.F. Fennell, R.E. Lopez, T. Nagai, *J. Geophys. Res. Sp. Phys.* **98**, 3815–3834 (1993). <https://doi.org/10.1029/92JA02475>
- L.F. Bargatze, D.N. Baker, R.L. McPherron, E.W. Hones, *J. Geophys. Res.* **90**, 6387 (1985). <https://doi.org/10.1029/JA090iA07p06387>
- W. Baumjohann, G. Paschmann, C.A. Cattell, *J. Geophys. Res. Sp. Phys.* **94**, 6597–6606 (1989). <https://doi.org/10.1029/ja094ia06p06597>
- W. Baumjohann, G. Paschmann, H. Lühr, *J. Geophys. Res.* **95**, 3801 (1990). <https://doi.org/10.1029/JA095iA04p03801>
- J. Birn, J.E. Borovsky, M. Hesse, K. Schindler, *Phys. Plasmas* **17**, 052108 (2010). <https://doi.org/10.1063/1.3429676>
- J. Birn, M. Hesse, *J. Geophys. Res. Sp. Phys.* **96**, 1611–1618 (1991). <https://doi.org/10.1029/90JA01762>
- J. Birn, M. Hesse, *Ann. Geophys.* **23**, 3365–3373 (2005). <https://doi.org/10.5194/angeo-23-3365-2005>
- J. Birn, M. Hesse, *J. Geophys. Res. Sp. Phys.* **118**, 3364–3376 (2013). <https://doi.org/10.1002/jgra.50187>
- J. Birn, M. Hesse, *J. Geophys. Res. Sp. Phys.* **119**, 3503–3513 (2014). <https://doi.org/10.1002/2014JA019863>
- J. Birn, M. Hesse, G. Haerendel, W. Baumjohann, K. Shiokawa, *J. Geophys. Res.* **104**, 19895 (1999). <https://doi.org/10.1029/1999JA900173>
- J. Birn, M. Hesse, S. Zenitani, *Phys. Plasmas* **18**, 111202 (2011a). <https://doi.org/10.1063/1.3626836>
- J. Birn, R. Nakamura, E.V. Panov, M. Hesse, *J. Geophys. Res. Sp. Phys.* **116**, A01210 (2011b). <https://doi.org/10.1029/2010JA016083>
- J. Birn, J. Raeder, Y.L. Wang, R.A. Wolf, M. Hesse, *Ann. Geophys.* **22**, 1773–1786 (2004). <https://doi.org/10.5194/angeo-22-1773-2004>
- R. Boström, *J. Geophys. Res.* **69**, 4983 (1964). <https://doi.org/10.1029/JZ069i023p04983>
- P.F. Bythrow, T.A. Potemra, *J. Geophys. Res.* **92**, 8691–8699 (1987). <https://doi.org/10.1029/JA092iA08p08691>
- C.X. Chen, R.A. Wolf, *J. Geophys. Res.* **98**, 21409–21419 (1993). <https://doi.org/10.1029/93JA02080>
- C.Z. Cheng, A.T.Y. Lui, *Geophys. Res. Lett.* **25**, 4091–4094 (1998). <https://doi.org/10.1029/1998GL900093>
- M. Connors, R.L. McPherron, B.J. Anderson, H. Korth, C.T. Russell, X. Chu, *Geophys. Res. Lett.* **41**, 4449–4455 (2014). <https://doi.org/10.1002/2014GL060604>
- F.V. Coroniti, P.L. Pritchett, *J. Geophys. Res. Sp. Phys.* **119**, 1827–1836 (2014). <https://doi.org/10.1002/2013JA01943>
- J.C. Coxon, S.E. Milan, L.B.N. Clausen, B.J. Anderson, H. Korth, *J. Geophys. Res. Sp. Phys.* **119**, 9804–9815 (2014). <https://doi.org/10.1002/2014JA020138>
- T.E. Cravens, *Physics of solar system plasmas* (Cambridge University Press, Cambridge, 1997)
- S.A. Cummer, R.R. Vondrak, R.F. Pfaff, J.W. Gjerloev, C.W. Carlson, R.E. Ergun, W.J. Peria, R.C. Elphic, R.J. Strangeway, J.B. Sigwarth, L.A. Frank, in *Magnetospheric Current Systems*, AGU

- Geophysical Monograph Series, ed. by Al S.-I. O., et al. (AGU, Washington, D. C., 2000), pp. 191–197
- H. Dahlgren, N. Ivchenko, B.S. Lanchester, M. Ashrafi, D. Whiter, G. Marklund, J. Sullivan **71**, 228–238 (2009). <https://doi.org/10.1016/j.jastp.2008.11.015>
- T.N. Davis, *J. Geophys. Res.* **67**, 75–110 (1962). <https://doi.org/10.1029/JZ067i001p00075>
- T.N. Davis, M. Sugiura, *J. Geophys. Res.* **71**, 785–801 (1966). <https://doi.org/10.1029/JZ071i003p00785>
- J.W. Dungey, *Phys. Rev. Lett.* **6**, 47–48 (1961). <https://doi.org/10.1103/PhysRevLett.6.47>
- Y. Ebihara, Simulation study of near-Earth space disturbances: 2. Auroral substorms. *Prog. Earth Planet. Sc.* **6**(1) (2019)
- Y. Ebihara, T. Tanaka, *J. Geophys. Res. A Sp. Phys.* **120**, 7270–7288 (2015a). <https://doi.org/10.1002/2015JA021516>
- Y. Ebihara, T. Tanaka, *J. Geophys. Res. Sp. Phys.* **120**, 10466–10484 (2015b). <https://doi.org/10.1002/2015JA021697>
- Y. Ebihara, T. Tanaka, *J. Geophys. Res. Sp. Phys.* **121**, 1201–1218 (2016). <https://doi.org/10.1002/2015JA021831>
- Y. Ebihara, T. Tanaka, *J. Geophys. Res. Sp. Phys.* **122**, 12288–12309 (2017). <https://doi.org/10.1002/2017JA024294>
- Y. Ebihara, T. Tanaka, *Plasma Phys. Control Fusion* (2018). <https://doi.org/10.1088/1361-6587/aa89fd>
- Y. Ebihara, T. Tanaka, N. Kamiyoshikawa, *J. Geophys. Res. Sp. Phys.* **124**, 360–378 (2019). <https://doi.org/10.1029/2018JA026177>
- Y. Ebihara, T. Tanaka, T. Kikuchi, *J. Geophys. Res. Sp. Phys.* **119**, 7281–7296 (2014). <https://doi.org/10.1002/2014JA020065>
- M. El-Alaoui, M. Ashour-Abdalla, R.J. Walker, V. Perroomian, R.L. Richard, V. Angelopoulos, A. Runov, *J. Geophys. Res. Sp. Phys.* **114**, A09204 (2009). <https://doi.org/10.1029/2009JA014133>
- L. Eliasson, R. Lundin, J.S. Murphree, *Geophys. Res. Lett.* **14**, 451–454 (1987). <https://doi.org/10.1029/GL014i004p00451>
- R.C. Elphic, J.W. Bonnell, R.J. Strangeway, L. Kepko, R.E. Ergun, J.P. McFadden, C.W. Carlson, W. Peria, C.A. Cattell, D. Klumpar, E. Shelley, W. Peterson, E. Moebius, L. Kistler, R. Pfaff, *Geophys. Res. Lett.* **25**, 2033–2036 (1998). <https://doi.org/10.1029/98GL01158>
- R.D. Elphinstone, D. Hearn, J.S. Murphree, L.L. Cogger, *J. Geophys. Res. Sp. Phys.* **96**, 1467–1480 (1991). <https://doi.org/10.1029/90JA01625>
- R.D. Elphinstone, D.J. Hearn, L.L. Cogger, J.S. Murphree, H. Singer, V. Sergeev, K. Mursula, D.M. Klumpar, G.D. Reeves, M. Johnson, *J. Geophys. Res.* **100**, 7937–7969 (1995a). <https://doi.org/10.1029/94JA02938>
- R.D. Elphinstone, D.J. Hearn, L.L. Cogger, J.S. Murphree, A. Wright, I. Sandahl, S. Ohtani, P.T. Newell, D.M. Klumpar, M. Shapshak, T.A. Potemra, K. Mursula, J.A. Sauvaud, *J. Geophys. Res.* **100**, 12093 (1995b). <https://doi.org/10.1029/95ja00327>
- D.H. Fairfield, N.F. Ness, *J. Geophys. Res.* **75**, 7032–7047 (1970). <https://doi.org/10.1029/JA075i034p07032>
- J.A. Fedder, S.P. Slinker, J.G. Lyon, R.D. Elphinstone, *J. Geophys. Res.* **100**, 19083 (1995). <https://doi.org/10.1029/95JA01524>
- J.A. Fedder, S.P. Slinker, J.G. Lyon, C.T. Russell, F.R. Fenrich, J.G. Luhmann, *Geophys. Res. Lett.* **24**, 2491–2494 (1997). <https://doi.org/10.1029/97GL02608>
- L.A. Frank, J.D. Craven, J.L. Burch, J.D. Winningham, *Geophys. Res. Lett.* **9**, 1001–1004 (1982). <https://doi.org/10.1029/GL009i009p01001>
- R. Fujii, R.A. Hoffman, P.C. Anderson, J.D. Craven, M. Sugiura, L.A. Frank, N.C. Maynard, *J. Geophys. Res.* **99**, 6093 (1994). <https://doi.org/10.1029/93JA02210>
- M. Fujimoto, I. Shinohara, H. Kojima, *Sp. Sci. Rev.* **160**, 123–143 (2011). <https://doi.org/10.1007/s11214-011-9807-7>
- H. Fukunishi, *J. Geophys. Res.* **80**, 553 (1975). <https://doi.org/10.1029/JA080i004p00553>
- X.C. Guo, C. Wang, Y.Q. Hu, J.R. Kan, *Geophys. Res. Lett.* **35**, 4–7 (2008). <https://doi.org/10.1029/2007GL032713>
- G. Haerendel, in *Proc. First Int. Conf. Substorms* (ESA Publications Division, Kiruna, 1992), pp. 417–420
- G. Haerendel, *J. Geophys. Res. Sp. Phys.* **112**, 1–21 (2007). <https://doi.org/10.1029/2007JA012378>
- G. Haerendel, *J. Geophys. Res.* **115**, 1–9 (2010). <https://doi.org/10.1029/2009JA015117>
- G. Haerendel, H.U. Frey, C.C. Chaston, O. Amm, L. Juusola, R. Nakamura, E. Seran, J.M. Weygand, *J. Geophys. Res. Sp. Phys.* **117**, 1–20 (2012). <https://doi.org/10.1029/2012JA018128>

- M. Hamrin, H. Gunell, J. Lindqvist, P.A. Lindqvist, R.E. Ergun, B.L. Giles, J. Geophys. Res. Sp. Phys. **123**, 242–258 (2018). <https://doi.org/10.1002/2017JA024826>
- M. Hamrin, T. Pitkänen, P. Norqvist, T. Karlsson, H. Nilsson, M. André, S. Buchert, A. Vaivads, O. Marghitsu, B. Klecker, L.M. Kistler, I. Dandouras, J. Geophys. Res. Sp. Phys. **119**, 9004–9018 (2014). <https://doi.org/10.1002/2014JA020285>
- H. Hasegawa, N. Ohno, T. Sato, J. Geophys. Res. Sp. Phys. (2010). <https://doi.org/10.1029/2009JA015093>
- M.G. Henderson, Ann. Geophys. **27**, 2129–2140 (2009). <https://doi.org/10.5194/angeo-27-2129-2009>
- M.G. Henderson, G.D. Reeves, J.S. Murphree, Geophys. Res. Lett. **25**, 3737–3740 (1998). <https://doi.org/10.1029/98GL02692>
- M. Hesse, J. Birn, J. Geophys. Res. **99**, 8565–8576 (1994). <https://doi.org/10.1029/94JA00441>
- E.W. Hones, Space Sci. Rev. **23**, 393–410 (1979). <https://doi.org/10.1007/BF00172247>
- E.W. Hones, J.R. Asbridge, S.J. Bame, S. Singer, J. Geophys. Res. **78**, 109–132 (1973). <https://doi.org/10.1029/JA078i001p00109>
- A. Ieda, K. Kauristie, Y. Nishimura, Y. Miyashita, H.U. Frey, L. Juusola, D. Whiter, M. Nosé, M.O. Fillingim, F. Honary, N.C. Rogers, Y. Miyoshi, T. Miura, T. Kawashima, S. Machida, Earth Planets Sp. (2018). <https://doi.org/10.1186/s40623-018-0843-3>
- T. Iijima, T.A. Potemra, J. Geophys. Res. **81**, 2165 (1976). <https://doi.org/10.1029/JA081i013p02165>
- S. Ismail, D.D. Wallis, L.L. Cogger, J. Geophys. Res. **82**, 4741–4749 (1977). <https://doi.org/10.1029/JA082i029p04741>
- F. Jiang, M. G. Kivelson, R. J. Strangeway, K. K. Khurana, R. Walker, 1–20 (2015) <https://doi.org/10.1002/2013JA019255>
- F. Jiang, R.J. Strangeway, M.G. Kivelson, J.M. Weygand, R.J. Walker, K.K. Khurana, Y. Nishimura, V. Angelopoulos, E. Donovan, J. Geophys. Res. Sp. Phys. **117**, 1–17 (2012). <https://doi.org/10.1029/2011JA017128>
- M.L. Johnson, J.S. Murphree, G.T. Marklund, T. Karlsson, J. Geophys. Res. Sp. Phys. **103**, 4271–4284 (1998). <https://doi.org/10.1029/97JA00854>
- A. Kadokura, A.S. Yukimatu, M. Ejiri, T. Oguti, M. Pinnock, M.R. Hairston, J. Geophys. Res. Sp. Phys. **107**, SSH4 (2002). <https://doi.org/10.1029/2001JA009127>
- Y. Kamide, S.-I. Akasofu, J. Geophys. Res. **80**, 3585–3602 (1975). <https://doi.org/10.1029/ja080i025p03585>
- Y. Kamide, S. Kokubun, J. Geophys. Res. Sp. Phys. **101**, 13027–13046 (1996). <https://doi.org/10.1029/96ja00142>
- Y. Kamide, A.D. Richmond, S. Matsushita, J. Geophys. Res. **86**, 801 (1981). <https://doi.org/10.1029/JA086iA02p00801>
- Y. Kamide, W. Sun, S.-I. Akasofu, J. Geophys. Res. **101**, 99 (1996). <https://doi.org/10.1029/95JA02990>
- J.R. Kan, R.L. Williams, S.-I. Akasofu, J. Geophys. Res. **89**, 2211 (1984). <https://doi.org/10.1029/JA089iA04p02211>
- A. Keiling, V. Angelopoulos, A. Runov, J. Weygand, S.V. Apatenkov, S. Mende, J. McFadden, D. Larson, O. Amm, K.H. Glassmeier, H.U. Auster, J. Geophys. Res. Sp. Phys. **114**, 1–11 (2009). <https://doi.org/10.1029/2009JA014114>
- L. Kepko, R.L. McPherron, O. Amm, S. Apatenkov, W. Baumjohann, J. Birn, M. Lester, R. Nakamura, T.I. Pulkkinen, V. Sergeev, Space Sci. Rev. **190**, 1–46 (2015). <https://doi.org/10.1007/s11214-014-0124-9>
- L. Kepko, E. Spanswick, V. Angelopoulos, E. Donovan, J. McFadden, K.-H. Glassmeier, J. Raeder, H.J. Singer, Geophys. Res. Lett. **36**, L24104 (2009). <https://doi.org/10.1029/2009GL041476>
- H. Korth, Y. Zhang, B.J. Anderson, T. Sotirelis, C.L. Waters, J. Geophys. Res. Sp. Phys. **119**, 6715–6731 (2014). <https://doi.org/10.1002/2014ja019961>
- H.E.J. Koskinen, E.I. Tanskanen, J. Geophys. Res. **107**, 1415 (2002). <https://doi.org/10.1029/2002JAO09283>
- K. Lassen, C. Danielsen, J. Geomagn. Geoelectr. **30**, 193–194 (1978). <https://doi.org/10.5636/jgg.30.193>
- K. Lassen, J.R. Sharber, J. D. Winningham **82**, 4741–4749 (1977). <https://doi.org/10.1029/JA082i032p05031>
- M.R. Lessard, W. Lotko, J. LaBelle, W. Peria, C.W. Carlson, F. Creutzberg, D.D. Wallis, J. Geophys. Res. Sp. Phys. **112**, 1–17 (2007). <https://doi.org/10.1029/2006JA011794>
- J. Liang, W.W. Liu, E. Spanswick, E.F. Donovan, J. Geophys. Res. Sp. Phys. **112**, A09209 (2007). <https://doi.org/10.1029/2007JA012354>
- C.S. Lin, R.A. Hoffman, Space Sci. Rev. **33**, 415–457 (1982). <https://doi.org/10.1007/BF00212420>

- W.W. Liu, J. Liang, E.F. Donovan, E. Spanswick, J. Geophys. Res. Sp. Phys. **117**, 1–12 (2012). <https://doi.org/10.1029/2012JA018161>
- M. Lockwood, C.J. Davis, *Ann. Geophys.* **17**, 178 (1999). <https://doi.org/10.1007/s005850050748>
- R.E. Lopez, J.G. Lyon, M.J. Wiltberger, C.C. Goodrich, *Adv. Sp. Res.* **28**, 1701–2001 (2001). [https://doi.org/10.1016/S0273-1177\(01\)00535-X](https://doi.org/10.1016/S0273-1177(01)00535-X)
- W. Lotko, A.V. Streltsov, C.W. Carlson, *Geophys. Res. Lett.* **25**, 4449–4452 (1998). <https://doi.org/10.1029/1998GL900200>
- G. Lu, D.N. Baker, R.L. McPherron, C.J. Farrugia, D. Lummerzheim, J.M. Ruohoniemi, F.J. Rich, D.S. Evans, R.P. Lepping, M. Brittnacher, X. Li, R. Greenwald, G. Sofko, J. Villain, M. Lester, J. Thayer, T. Moretto, D. Milling, O. Troshichev, A. Zaitzev, V. Odintsov, G. Makarov, K. Hayashi, J. Geophys. Res. Sp. Phys. **103**, 11685–11694 (1998). <https://doi.org/10.1029/98JA00897>
- A.T.Y. Lui, J. Geophys. Res. Sp. Phys. **101**, 13067–13088 (1996). <https://doi.org/10.1029/96JA00079>
- A.T.Y. Lui, J. Geophys. Res. Sp. Phys. **116**, A01210 (2011). <https://doi.org/10.1029/2011JA017107>
- A.T.Y. Lui, J.R. Burrows, J. Geophys. Res. Sp. Phys. **83**, 3342–3348 (1978). <https://doi.org/10.1029/JA083iA07p03342>
- A.T.Y. Lui, C.-L. Chang, A. Mankofsky, H.-K. Wong, D. Winske, J. Geophys. Res. **96**, 11389 (1991). <https://doi.org/10.1029/91JA00892>
- J.G. Lyon, R.E. Lopez, C.C. Goodrich, M. Wiltberger, K. Papadopoulos, *Geophys. Res. Lett.* **25**, 3039–3042 (1998). <https://doi.org/10.1029/98GL00662>
- L.R. Lyons, D.S. Evans, R. Lundin, J. Geophys. Res. **84**, 457–461 (1979). <https://doi.org/10.1029/JA084iA02p00457>
- L.R. Lyons, Y. Nishimura, H.-J. Kim, E. Donovan, V. Angelopoulos, G. Sofko, M. Nicolls, C. Heinselman, J.M. Ruohoniemi, N. Nishitani, J. Geophys. Res. **116**, A12225 (2011). <https://doi.org/10.1029/2011JA016850>
- L.R. Lyons, Y. Nishimura, Y. Shi, S. Zou, H.-J. Kim, V. Angelopoulos, C. Heinselman, M.J. Nicolls, K.-H. Fornacon, J. Geophys. Res. **115**, A07223 (2010). <https://doi.org/10.1029/2009JA015168>
- L.R. Lyons, J.C. Samson, *Geophys. Res. Lett.* **19**, 2171–2174 (1992). <https://doi.org/10.1029/92GL02494>
- R.L. Lysak, C.T. Dum, J. Geophys. Res. **88**, 365 (1983). <https://doi.org/10.1029/JA088iA01p00365>
- R.L. Lysak, Y. Song, J. Geophys. Res. Sp. Phys. **107**, SIA 6-1–SIA 6-13 (2002). <https://doi.org/10.1029/2001JA000308>
- S. Machida, Y. Miyashita, A. Ieda, M. Nosé, V. Angelopoulos, J.P. McFadden, *Ann. Geophys.* **32**, 99–111 (2014). <https://doi.org/10.5194/angeo-32-99-2014>
- S. Machida, Y. Miyashita, A. Ieda, M. Nosé, D. Nagata, K. Liou, T. Obara, A. Nishida, Y. Saito, T. Mukai, *Ann. Geophys.* **27**, 1035–1046 (2009). <https://doi.org/10.5194/angeo-27-1035-2009>
- O. Marghitsu, M. Hamrin, B. Klecker, A. Vaivads, J. McFadden, S. Buchert, L.M. Kistler, I. Dandouras, M. André, H. Rème, *Ann. Geophys.* **24**, 619–635 (2006). <https://doi.org/10.5194/angeo-24-619-2006>
- G. Marklund, *Planet. Space Sci.* **32**, 193–211 (1984). [https://doi.org/10.1016/0032-0633\(84\)90154-5](https://doi.org/10.1016/0032-0633(84)90154-5)
- G.T. Marklund, T. Karlsson, L.G. Blomberg, P.-A. Lindqvist, C.-G. Fälthammar, M.L. Johnson, J.S. Murphree, L. Andersson, L. Eliasson, H.J. Opgenoorth, L.J. Zanetti, J. Geophys. Res. **103**, 4125–4144 (1998). <https://doi.org/10.1029/97JA00558>
- R.L. McPherron, J. Geophys. Res. **75**, 5592–5599 (1970). <https://doi.org/10.1029/JA075i028p05592>
- R.L. McPherron, *Planet. Space Sci.* **20**, 1521–1539 (1972). [https://doi.org/10.1016/0032-0633\(72\)90054-2](https://doi.org/10.1016/0032-0633(72)90054-2)
- R.L. McPherron, C.T. Russell, M.P. Aubry, J. Geophys. Res. **78**, 3131–3149 (1973). <https://doi.org/10.1029/JA078i016p03131>
- S.B. Mende, J. Geophys. Res. **108**, 8010 (2003). <https://doi.org/10.1029/2002JA009413>
- S.B. Mende, H.U. Frey, V. Angelopoulos, Y. Nishimura, J. Geophys. Res. Sp. Phys. **116**, A00131 (2011). <https://doi.org/10.1029/2010JA015733>
- C.-I. Meng, J. Geophys. Res. **81**, 2771–2785 (1976). <https://doi.org/10.1029/JA081i016p02771>
- C.-I. Meng, R. Lundin, J. Geophys. Res. **91**, 1572 (1986). <https://doi.org/10.1029/JA091iA02p01572>
- C.-I. Meng, A.L. Snyder, H.W. Kroehl, J. Geophys. Res. **83**, 575 (1978). <https://doi.org/10.1029/JA083iA02p00575>
- Y. Miyashita, S. Machida, Y. Kamide, D. Nagata, K. Liou, M. Fujimoto, A. Ieda, M.H. Saito, C.T. Russell, S.P. Christon, M. Nosé, H.U. Frey, I. Shinohara, T. Mukai, Y. Saito, H. Hayakawa, J. Geophys. Res. Sp. Phys. **114**, A01211 (2009). <https://doi.org/10.1029/2008JA013225>
- F.S. Mozer, C.A. Cattell, M.K. Hudson, R.L. Lysak, M. Temerin, R.B. Torbert, *Sp. Sci. Rev.* **27**, 155–213 (1980). <https://doi.org/10.1007/BF00212238>

- F.S. Mozer, A. Hull, *J. Geophys. Res.* **106**, 5763 (2001). <https://doi.org/10.1029/2000JA900117>
- T. Nagai, M. Fujimoto, Y. Saito, S. Machida, T. Terasawa, R. Nakamura, T. Yamamoto, T. Mukai, A. Nishida, S. Kokubun, *J. Geophys. Res. Sp. Phys.* **103**, 4419–4440 (1998). <https://doi.org/10.1029/97JA02190>
- T. Nagai, I. Shinohara, M. Fujimoto, S. Machida, R. Nakamura, Y. Saito, T. Mukai, *J. Geophys. Res. Sp. Phys.* **108**, 1–8 (2003). <https://doi.org/10.1029/2003JA009900>
- R. Nakamura, T. Oguti, T. Yamamoto, S. Kokubun, *J. Geophys. Res. Sp. Phys.* **98**, 5743–5759 (1993). <https://doi.org/10.1029/92ja02230>
- P.T. Newell, D. Xu, C.-I. Meng, M.G. Kivelson, *J. Geophys. Res. Sp. Phys.* **102**, 127–139 (1997). <https://doi.org/10.1029/96JA03045>
- A. Nishida, *Sp. Sci. Rev.* **34**, 185–200 (1983). <https://doi.org/10.1007/BF00194626>
- A. Nishida, K. Fujii, *Planet. Sp. Sci.* **24**, 849–853 (1976). [https://doi.org/10.1016/0032-0633\(76\)90075-1](https://doi.org/10.1016/0032-0633(76)90075-1)
- A. Nishida, J. Hones, *J. Geophys. Res.* **79**, 535 (1974). <https://doi.org/10.1029/JA079i004p00535>
- A. Nishida, Y. Kamide, *J. Geophys. Res.* **88**, 7005–7014 (1983)
- A. Nishida, N. Nagayama, *J. Geophys. Res.* **78**, 3782–3798 (1973). <https://doi.org/10.1029/JA078i019p03782>
- Y. Nishimura, L. Lyons, S. Zou, V. Angelopoulos, S. Mende, O. Sciences, L. Angeles, P. Physics, O. Sciences, S. Sciences, A. Arbor, *J. Geophys. Res.* **115**, A07222 (2010a). <https://doi.org/10.1029/2009J A015166>
- Y. Nishimura, L.R. Lyons, T. Kikuchi, V. Angelopoulos, E.F. Donovan, S.B. Mende, H. Lühr, *Geophys. Res. Lett.* **39**, L22101 (2012). <https://doi.org/10.1029/2012GL053761>
- Y. Nishimura, L.R. Lyons, S. Zou, X. Xing, V. Angelopoulos, S.B. Mende, J.W. Bonnell, D. Larson, U. Auster, T. Hori, N. Nishitani, K. Hosokawa, G. Sofko, M. Nicolls, C. Heinselman, *J. Geophys. Res.* **115**, A00I08 (2010b). <https://doi.org/10.1029/2010JA015832>
- Y. Nishimura, J. Yang, P.L. Pritchett, F.V. Coroniti, E.F. Donovan, L.R. Lyons, R.A. Wolf, V. Angelopoulos, S.B. Mende, *J. Geophys. Res. Sp. Phys.* **121**, 8661–8676 (2016). <https://doi.org/10.1002/2016J A022801>
- T. Ogawa, T. Sato, *Planet. Space Sci.* **19**, 1393–1412 (1971). [https://doi.org/10.1016/0032-0633\(71\)90001-8](https://doi.org/10.1016/0032-0633(71)90001-8)
- T. Oguti, *J. Geophys. Res.* **78**, 7543–7547 (1973). <https://doi.org/10.1029/JA078i031p07543>
- S. Ohtani, H. Korth, S. Wing, E.R. Talaat, H.U. Frey, J.W. Gjerloev, *J. Geophys. Res. Sp. Phys.* **117**, 1–26 (2012). <https://doi.org/10.1029/2011JA017501>
- A. Olsson, M.A.L. Persson, H.J. Oppenorth, S. Kirkwood, *J. Geophys. Res.* **101**, 24661 (1996). <https://doi.org/10.1029/96JA01748>
- H.J. Oppenorth, M.A.L. Persson, T.I. Pulkkinen, R.J. Pellinen, *J. Geophys. Res. Sp. Phys.* **99**, 4115–4129 (1994). <https://doi.org/10.1029/93JA01502>
- N. Østgaard, *J. Geophys. Res.* **107**, 1233 (2002). <https://doi.org/10.1029/2001JA002002>
- M. Palmroth, P. Janhunen, G. Germany, D. Lummerzheim, K. Liou, D.N. Baker, C. Barth, A.T. Weatherwax, J. Watermann, *Ann. Geophys.* **24**, 861–872 (2006). <https://doi.org/10.5194/angeo-24-861-2006>
- M. Palmroth, P. Janhunen, T.I. Pulkkinen, A. Aksnes, G. Lu, N. Østgaard, J. Watermann, G.D. Reeves, G.A. Germany, *Ann. Geophys.* **23**, 2051–2068 (2005). <https://doi.org/10.5194/angeo-23-2051-2005>
- M. Palmroth, P. Janhunen, T.I. Pulkkinen, H.E.J. Koskinen, *Ann. Geophys.* **22**, 549–566 (2004). <https://doi.org/10.5194/angeo-22-549-2004>
- K. Papadopoulos, C. Goodrich, M. Wiltberger, R. Lopez, J.G. Lyon, *Phys. Chem. Earth Part C Solar Terr. Planet. Sci.* **24**, 189–202 (1999). [https://doi.org/10.1016/S1464-1917\(98\)00028-2](https://doi.org/10.1016/S1464-1917(98)00028-2)
- P. Perreault, S.-I. Akasofu, *Geophys. J. Int.* **54**, 547–573 (1978). <https://doi.org/10.1111/j.1365-246X.1978.tb05494.x>
- D.H. Pontius, R.A. Wolf, *Geophys. Res. Lett.* **17**, 49–52 (1990). <https://doi.org/10.1029/GL017i001p00049>
- I.J. Rae, C.E.J. Watt, I.R. Mann, K.R. Murphy, J.C. Samson, K. Kabin, V. Angelopoulos, *J. Geophys. Res. Sp. Phys.* **115**, 1–10 (2010). <https://doi.org/10.1029/2010JA015376>
- J. Raeder, R.L. McPherron, L.A. Frank, S. Kokubun, G. Lu, T. Mukai, W.R. Paterson, J.B. Sigwarth, H.J. Singer, J.A. Slavin, *J. Geophys. Res. Sp. Phys.* **106**, 381–395 (2001). <https://doi.org/10.1029/2000J A000605>
- J. Raeder, P. Zhu, Y. Ge, G. Siscoe, *J. Geophys. Res.* **115**, A00I16 (2010a). <https://doi.org/10.1029/2010j a015876>

- J. Raeder, P. Zhu, Y. Ge, G. Siscoe, J. Geophys. Res. Sp. Phys. **115**, A10225 (2010b). <https://doi.org/10.1029/2010JA015876>
- J. Raeder, P. Zhu, Y. Ge, G. Siscoe, Auror Phenomenol. Magnetos. Process Earth Other Planet **197**, 389–395 (2012)
- R. Rankin, J.C. Samson, V.T. Tikhonchuk, Geophys. Res. Lett. **26**, 3601–3604 (1999). <https://doi.org/10.1029/1999GL010715>
- J.B. Ream, R.J. Walker, M. Ashour-Abdalla, M. El-Alaoui, M.G. Kivelson, M.L. Goldstein, J. Geophys. Res. Sp. Phys. **118**, 6364–6377 (2013). <https://doi.org/10.1002/2013JA018734>
- H. Rème, J.M. Bosqued, J. Geophys. Res. **78**, 5553–5558 (1973). <https://doi.org/10.1029/JA078i025p05553>
- P. Ricci, J.U. Brackbill, W. Daughton, G. Lapenta, Phys. Plasmas **11**, 4489–4500 (2004). <https://doi.org/10.1063/1.1778744>
- A.D. Richmond, Y. Kamide, S.-I. Akasofu, D. Alcaydé, M. Blanc, O. de la Beaujardière, D.S. Evans, J.C. Foster, E. Friis-Christensen, J.M. Holt, R.J. Pellinen, C. Senior, A.N. Zaitzev, J. Geophys. Res. **95**, 1061 (1990). <https://doi.org/10.1029/JA095iA02p01061>
- G. Rostoker, S.I. Akasofu, J. Foster, R.A. Greenwald, Y. Kamide, K. Kawasaki, A.T.Y. Lui, R.L. McPherron, C.T. Russell, J. Geophys. Res. **85**, 1663–1668 (1980). <https://doi.org/10.1029/JA085iA04p01663>
- G. Rostoker, J.C. Armstrong, A.J. Zmuda, J. Geophys. Res. **80**, 3571–3579 (1975). <https://doi.org/10.1029/JA080i025p03571>
- P.L. Rothwell, M.B. Silevitch, L.P. Block, J. Geophys. Res. **89**, 8941 (1984). <https://doi.org/10.1029/JA089iA10p08941>
- P.L. Rothwell, M.B. Silevitch, L.P. Block, P. Tanskanen, J. Geophys. Res. **93**, 8613 (1988). <https://doi.org/10.1029/JA093iA08p08613>
- A. Roux, S. Perraut, P. Robert, A. Morane, A. Pedersen, A. Korth, G. Kremser, B. Aparicio, D. Rodgers, R. Pellinen, J. Geophys. Res. **96**, 17697 (1991). <https://doi.org/10.1029/91JA01106>
- H.L. Rowland, P.J. Palmadesso, J. Geophys. Res. **88**, 7997 (1983). <https://doi.org/10.1029/JA088iA10p07997>
- O. Royrvik, T.N. Davis, J. Geophys. Res. **82**, 4720 (1977). <https://doi.org/10.1029/JA082i029p04720>
- K. Sakaguchi, K. Shiokawa, E. Donovan, Geophys. Res. Lett. **36**, 2–6 (2009). <https://doi.org/10.1029/2009GL041252>
- T. Sakanoi, H. Fukunishi, T. Mukai, J. Geophys. Res. **100**, 19343–19360 (1995)
- T. Sato, J. Geophys. Res. Sp. Phys. **83**, 1042–1048 (1978). <https://doi.org/10.1029/JA083iA03p01042>
- T. Sato, T. Iijima, Sp. Sci. Rev. **24**, 347–366 (1979). <https://doi.org/10.1007/BF00212423>
- V. Sergeev, V. Angelopoulos, M. Kubyshkina, E. Donovan, X.Z. Zhou, A. Runov, H. Singer, J. McFadden, R. Nakamura, J. Geophys. Res. Sp. Phys. **116**, A00I26 (2011). <https://doi.org/10.1029/2010J A015689>
- V.A. Sergeev, J.A. Sauvaud, D. Popescu, R.A. Kovrazhkin, K. Liou, P.T. Newell, M. Brittner, G. Parks, R. Nakamura, T. Mukai, G.D. Reeves, Geophys. Res. Lett. **27**, 851–854 (2000). <https://doi.org/10.1029/1999GL010729>
- V.A. Sergeev, P. Tanskanen, K. Mursula, A. Korth, R.C. Elphic, J. Geophys. Res. **95**, 3819 (1990). <https://doi.org/10.1029/JA095iA04p03819>
- K. Shiokawa, W. Baumjohann, G. Haerendel, Geophys. Res. Lett. **24**, 1179 (1997a). <https://doi.org/10.1029/97GL01062>
- K. Shiokawa, H. Fukunishi, J. Geomagn. Geoelectr. **43**, 691–719 (1991). <https://doi.org/10.5636/jgg.43.691>
- K. Shiokawa, T. Ogino, K. Hayashi, D.J. McEwen, J. Geophys. Res. **102**, 24325 (1997b). <https://doi.org/10.1029/97JA02383>
- K. Shiokawa, K. Yumoto, K. Hayashi, T. Oguti, D.J. McEwen, J. Geophys. Res. **100**, 21979 (1995). <https://doi.org/10.1029/95JA01564>
- K.D. Siebert, G.L. Siscoe, J. Geophys. Res. Sp. Phys. **107**, 1095 (2002). <https://doi.org/10.1029/2001J A000237>
- G.L. Siscoe, W.D. Cummings, Planet. Sp. Sci. **17**, 1795–1802 (1969). [https://doi.org/10.1016/0032-0633\(69\)90055-5](https://doi.org/10.1016/0032-0633(69)90055-5)
- G.L. Siscoe, K.D. Siebert, J. Atmos. Solar-Terr. Phys. **68**, 911–920 (2006). <https://doi.org/10.1016/j.jastp.2005.11.012>
- S.P. Slinker, J.A. Fedder, J.M. Ruohoniemi, J.G. Lyon, J. Geophys. Res. Sp. Phys. **106**, 361–380 (2001). <https://doi.org/10.1029/2000JA000603>

- M.V. Stepanova, E.E. Antonova, J.M. Bosqued, R.A. Kovrazhkin, K.R. Aubel, J. Geophys. Res. Sp. Phys. **107**, A7 (2002). <https://doi.org/10.1029/2001JA003503>
- A. Streltsov, W. Lotko, J. Geophys. Res. **100**, 19457 (1995). <https://doi.org/10.1029/95JA01553>
- W. Sun, B.H. Ahn, S.I. Akasofu, Planet. Space Sci. **33**, 279–281 (1985). [https://doi.org/10.1016/0032-0633\(85\)90059-5](https://doi.org/10.1016/0032-0633(85)90059-5)
- D.W. Swift, Rev. Geophys. **19**, 185 (1981). <https://doi.org/10.1029/RG019i001p00185>
- T. Tanaka, J. Comput. Phys. **111**, 381–389 (1994). <https://doi.org/10.1006/jcph.1994.1071>
- T. Tanaka, J. Geophys. Res. **100**, 12057–12074 (1995). <https://doi.org/10.1029/95JA00419>
- T. Tanaka, J. Geophys. Res. Sp. Phys. **105**, 21081–21096 (2000). <https://doi.org/10.1029/2000JA900061>
- T. Tanaka, *Magnetosphere-Ionosphere Convection as a Compound System* (Springer, Berlin, 2007)
- T. Tanaka, *Auror Dynamics Space Weather* (Wiley, Hoboken, 2015), pp. 177–190
- T. Tanaka, Y. Ebihara, M. Watanabe, M. Den, S. Fujita, T. Kikuchi, K.K. Hashimoto, R. Kataoka, J. Geophys. Res. Sp. Phys. **122**, 6210–6239 (2017). <https://doi.org/10.1002/2017JA024102>
- T. Tanaka, A. Nakamizo, A. Yoshikawa, S. Fujita, H. Shinagawa, H. Shimazu, T. Kikuchi, K.K. Hashimoto, J. Geophys. Res. Sp. Phys. **115**, A05220 (2010). <https://doi.org/10.1029/2009JA014676>
- T. Tanaka, M. Watanabe, M. Den, S. Fujita, Y. Ebihara, T. Kikuchi, K.K. Hashimoto, R. Kataoka, Generation of field-aligned current (FAC) and convection through the formation of pressure regimes: Correction for the concept of Dungey's convection. J. Geophys. Res. Space Phys. **121**(9), 8695–8711 (2016)
- E. Tanskanen, T.I. Pulkkinen, H.E.J. Koskinen, J.A. Slavin, J. Geophys. Res. **107**, 1086 (2002). <https://doi.org/10.1029/2001JA900153>
- R.A. Treumann, Earth Planets Sp. **53**, 453–462 (2001). <https://doi.org/10.1186/BF03353256>
- R.A. Treumann, C.H. Jaroschek, R. Nakamura, A. Runov, M. Scholer, Adv. Sp. Res. **38**, 101–111 (2006). <https://doi.org/10.1016/j.asr.2004.11.045>
- V.M. Vasyliunas, J.R. Kan, G.L. Siscoe, S.-I. Akasofu, Planet. Space Sci. **30**, 359–365 (1982). [https://doi.org/10.1016/0032-0633\(82\)90041-1](https://doi.org/10.1016/0032-0633(82)90041-1)
- K. Watanabe, M. Ashour-Abdalla, T. Sato, J. Geophys. Res. **91**, 6973 (1986). <https://doi.org/10.1029/JA091iA06p06973>
- M. Watanabe, T. Tanaka, S. Fujita, J. Geophys. Res. Sp. Phys. (2019). <https://doi.org/10.1029/2018JA026025>
- D.R. Weimer, J. Geophys. Res. Sp. Phys. **110**, 1–21 (2005). <https://doi.org/10.1029/2004JA010884>
- D.R. Weimer, J.D. Craven, L.A. Frank, W.B. Hanson, N.C. Maynard, R.A. Hoffman, J.A. Slavin, J. Geophys. Res. **99**, 23639 (1994). <https://doi.org/10.1029/94JA01976>
- D.R. Weimer, D.A. Gurnett, C.K. Goertz, J.D. Menietti, J.L. Burch, M. Sugiura, J. Geophys. Res. **92**, 187 (1987). <https://doi.org/10.1029/JA092iA01p00187>
- M. Wiltberger, T.I. Pulkkinen, J.G. Lyon, C.C. Goodrich, J. Geophys. Res. **105**, 27649 (2000). <https://doi.org/10.1029/1999JA000251>
- M. Wiltberger, R.S. Weigel, W. Lotko, J.A. Fedder, J. Geophys. Res. Sp. Phys. **114**, 1–11 (2009). <https://doi.org/10.1029/2008JA013108>
- A.N. Wright, J. Geophys. Res. Sp. Phys. **101**, 13169–13178 (1996). <https://doi.org/10.1029/96JA00541>
- A.G. Yahnin, V.A. Sergeev, B.B. Gvozdevsky, S. Vennerstrøm, Ann. Geophys. **15**, 943–958 (1997). <https://doi.org/10.1007/s00585-997-0943-z>
- Y. Yao, Y. Ebihara, T. Tanaka, J. Geophys. Res. Sp. Phys. **120**, 201–211 (2015a). <https://doi.org/10.1002/2014JA020482>
- Y. Yao, Y. Ebihara, T. Tanaka, J. Geophys. Res. Sp. Phys. **120**, 6427–6435 (2015b). <https://doi.org/10.1002/2015JA021187>
- Z.H. Yao, Z.Y. Pu, S.Y. Fu, V. Angelopoulos, M. Kubyshkina, X. Xing, L. Lyons, Y. Nishimura, L. Xie, X.G. Wang, C.J. Xiao, X. Cao, J. Liu, H. Zhang, M. Nowada, Q.G. Zong, R.L. Guo, J. Zhong, J.X. Li, Geophys. Res. Lett. (2012). <https://doi.org/10.1029/2012GL052055>
- E. Zesta, L.R. Lyons, E. Donovan, Geophys. Res. Lett. **27**, 3241–3244 (2000). <https://doi.org/10.1029/2000GL000027>
- X.-Y. Zhou, W. Sun, A.J. Ridley, S.B. Mende, J. Geophys. Res. Sp. Phys. **116**, A00I28 (2011). <https://doi.org/10.1029/2010JA015804>